

Return of the CHAMPs: A clockwork portal to charged dark matter

Debajyoti Choudhury,^a Vineet K. Jha,^a Suvam Maharana^b

^a*Department of Physics and Astrophysics, University of Delhi, Delhi 110 007, India.*

^b*Department of Theoretical Physics, Tata Institute of Fundamental Research, Homi Bhabha Road, Mumbai 400005, India.*

E-mail: vineet.phd2022@physics.du.ac.in

ABSTRACT: While Dark Matter (DM) is conventionally assumed to be chargeless, the possibility of a charged massive particle (CHAMP) as the DM particle remains alive. With phenomenological constraints on the charge being very severe, such a scenario is often sought to be dismissed, citing naturalness. We demonstrate here that such a (mini)charged DM can be realized within the clockwork paradigm, without the need to invoke unnaturally small parameters. The model is examined against constraints, theoretical and experimental, and the phenomenologically admissible parameter space is delineated. Several intriguing tests, at the LHC as well as at future direct and indirect detection experiments, are pointed out.

Contents

1	Introduction	1
2	Model	4
2.1	Clockwork with vector fields	4
2.2	The clockwork extended SM	7
3	Constraints	11
3.1	Theoretical constraints	12
3.2	Experimental constraints	14
3.2.1	Electroweak Constraints	14
3.2.2	Direct detection constraints	17
3.2.3	Collider Bounds	20
4	Dark matter phenomenology	22
4.1	The simplest scenario: $\chi\bar{\chi} \rightarrow \psi\bar{\psi}$	22
4.2	Including all annihilation channels	25
4.2.1	$\chi\bar{\chi} \rightarrow Z'_k Z'_l$	25
4.2.2	$\chi\bar{\chi} \rightarrow Z'_k \varphi_n, Z'_k \Phi$	26
5	Summary and Discussion	27

1 Introduction

The nature of dark matter (DM) in the observable Universe still remains frustratingly obscure. While its existence (and its overwhelming contribution to the matter-energy density of the Universe) can be inferred from its gravitational interactions, very little is known about the properties of the DM particle, whether it be its mass or spin, or its participation in the other known fundamental interactions. The standard strong interactions are disfavoured, as that would lead to stable exotic bound states, and no such states have been seen. Similarly, strong self-interactions would, nominally, lead to significant pressure for a DM cloud, thereby interfering with large-scale structure formation. Nonetheless, certain assertions with regards the DM's mass and its possible interactions with the visible sector are often made from a purely phenomenological point of view. Although these assumptions may not necessarily have a strong theoretical or observational motivation, they appear to be the most natural choices within minimal extensions of the Standard Model (SM) and, therefore, prove to be essential testing grounds for DM model-building. One such assertion is that of a weak-scale [$\sim \mathcal{O}(100 \text{ GeV} - 1 \text{ TeV})$] DM, a natural possibility considering that the fundamental scale of the visible sector is *presumably* set by electroweak symmetry breaking

(EWSB). Of course, this is already otherwise motivated from the fact that a weak-scale DM interacting with visible matter through a weak-strength coupling automatically produces the correct thermal relic abundance in the Universe — the so-called WIMP miracle. Then, for the simplest case of a weak-isospin singlet DM, minimalism dictates that nongravitational DM-SM interactions can exist either through the Higgs portal or through the Z portal. Note, though, that if the DM is indeed a SM-singlet, the gauge-invariant completion of the required DM- Z interactions can only be furnished by higher-dimensional operators involving DM couplings with the Higgs doublet and its covariant derivative [1, 2]. However, the DM-SM couplings dictating the thermal freeze-out relic as well as the DM-nucleon scatterings in both these minimal portals have largely been ruled out for a weak-scale DM by negative results in direct detection experiments¹ (see *e.g.* ref.[4]).

Although relatively less explored for a heavy relic, it is possible in general that it carries a nonzero electric charge, most naturally through a nonzero hypercharge. Such electrically CHArged Massive Particles (CHAMPs) were originally proposed in ref.[5] with the assumption that they carry unit or integral charges and were subsequently reexamined in ref. [6] for fractional charges as well. Expectedly, CHAMP candidates with integral charges were soon ruled out by the nonobservation of heavy exotic atoms as well as from direct searches [7].

Studied extensively for light DM candidates (see *e.g.* refs. [8–11]), fractionally charged particles (with the charge being parametrized as $Q_{DM} = \epsilon e$), too, are subject to strong cosmological, astrophysical, and terrestrial constraints [12]. For instance, the suppression of invisible decay modes of the ortho-positronium requires $\epsilon \lesssim 10^{-5}$ for $m_{DM} < m_e$ [13]. Similarly, the SLAC accelerator experiment places upper limits of $\epsilon \lesssim 4.1 \times 10^{-5}$ for particles with mass around 1 MeV and $\epsilon \lesssim 5.8 \times 10^{-4}$ for particles with mass around 100 MeV [14]. Stellar constraints are particularly stringent for $m_{DM} \lesssim 10$ keV, from plasmon decays into such particles, with the strongest bounds ($\epsilon \lesssim 10^{-14}$) emanating from observations of low-mass red giants and white dwarfs [12, 15]. Analogously, if they were relativistic during the epoch of big bang nucleosynthesis (BBN) —*i.e.*, $m_{DM} \lesssim \mathcal{O}(\text{MeV})$ — they would impact the expansion rate of the universe during BBN, and hence the synthesis of light elements (while the effective number of relativistic species is predicted to be $N_{\text{eff}} = 3.046$ within the SM, current Planck results constrain it to $N_{\text{eff}} = 2.99 \pm 0.17$ [16]).

It was argued in ref.[17] that the constraints emanating from terrestrial experiments may be relaxed by exploiting the possibility that the halo CHAMPs are either stopped from penetrating the galactic disk by its magnetic field or are expelled due to interactions with supernovae remnants, provided the CHAMP masses fall in the range $100(Q_{DM}/e)^2 \text{ TeV} \lesssim m_{DM} \lesssim 10^8(Q_{DM}/e) \text{ TeV}$. Consequently, a heavy CHAMP possessing a tiny Q_{DM} is not subject to such expulsions, and for the scenario where it saturates the DM abundance, the present-day direct detection experiments place the most stringent upper bounds on its electric charge, namely $Q_{DM} \lesssim 10^{-10}e$, for $m_{DM} \lesssim 10^5 \text{ GeV}$ [18–20].

From a model-building perspective, then, it becomes a challenge to naturally invoke

¹Assuming a nonstandard cosmology, however, may still render a region of the parameter space of these models viable [3].

such a tiny charge for the CHAMP. A quasi-phenomenological route would be to posit a dark sector composed of particles charged under a new Abelian gauge group $U(1)_C$. If the corresponding gauge boson (the dark photon C_μ) kinetically mixes with the SM hypercharge boson (B_μ) through a term $\epsilon B_{\mu\nu}C^{\mu\nu}$, it can result in the new particle(s) acquiring an effective electric charge proportional to the mixing parameter ϵ . The smallness of ϵ is sought to be explained by requiring it to appear only through radiative corrections, to be engendered by introducing particles that carry both $U(1)_Y$ and $U(1)_C$ charges. However, restricting $Q_{DM} \lesssim 10^{-10}e$ requires a large suppression in the kinetic mixing, which can be realized if it is induced only at an adequately high loop order [21], typically necessitating the introduction of new symmetries and/or multiple new fields².

In this work, we construct, instead, a model wherein the tiny charge is generated via a localization of the SM photon in a theory space. Appealing to the clockwork (CW) paradigm [25–28], we enlarge the Abelian factor of the SM gauge group as $U(1)_Y \rightarrow U(1)^{N+1}$. A spontaneous breaking of the symmetry at a scale $f \gg m_{EW}$ by N link scalars Φ_j (with unequal charges Q_{j+1} and Q_j under adjacent $U(1)$'s) then leads to a theory of Abelian gauge bosons with nearest-neighbour mass terms. With one subgroup $U(1)_{CW}$ remaining unbroken, the vector boson spectrum contains a massless particle along with a tower of heavy partners with masses $\sim gqf$, where g denotes the universal gauge coupling of the $U(1)$'s and q defines the ratio $|Q_{j+1}/Q_j|$. As long as $q \gtrsim 2$, the clockwork mechanism dictates that the massless vector field, which can be identified with the SM hypercharge field B_μ , is localized near the 0-th site on the theory space lattice. Consequently, if the CHAMP χ is assumed to be charged only under $U(1)_N$, it would possess a coupling with B_μ that is suppressed by an exponential factor $\sim q^{-N}$. On the other hand, if the SM fermions and the Higgs field are charged under $U(1)_0$ with the same quantum numbers as the standard hypercharge assignments, their coupling with B_μ can, in principle, be commensurate with the SM values.

Understandably, phenomenological consistency constrains the *a priori* free parameters of the clockwork sector, namely q , N and g . For instance, the experimental constraint on the CHAMP's electric charge correlates q and N , whereas the value of the gauge coupling g (chosen, *for simplicity*, to have a uniform value over the lattice) is fixed by demanding that the photon and the Z couplings to visible matter are precisely SM-like. The spontaneous symmetry breaking (SSB) scale f , which also specifies the masses of the heavy CW vector bosons (the harbingers of a set of Z 's) as well as the link scalars, is bounded from below by the current collider limits on the masses of neutral gauge bosons as well as the electroweak precision observables. Interestingly, the Z 's play a pivotal role in setting the relic abundance of the CHAMP DM candidate (which remains a problem in a stand-alone CHAMP theory with such a small ϵ) through the freeze-out mechanism. We find that in our minimal and constrained setup, with the CHAMP being a Dirac fermion, the primary annihilation channel for χ is $\chi\bar{\chi} \rightarrow f\bar{f}$, where f denotes the SM fermions, and mediated by the Z 's.

²A kinetic mixing of such a small magnitude could possibly be induced within string theoretic/extrdimensional setups as well, see *e.g* refs.[22–24]. However, from an effective four-dimensional point of view, these too, in some form, would appear to be elaborate constructions comprising multiple new degrees of freedom (at least a spectrum of gravitons).

The correct relic abundance is most easily obtained when $m_\chi \sim m_{Z'}/2$. Since electroweak precision and the prevailing collider constraints push the lower limit on the Z' mass scale in the model to the multi-TeV range, the allowed DM mass is also accordingly restricted to be around or above the TeV scale. Thus, for f near the TeV scale, the model naturally accommodates a minicharged CHAMP DM of mass in the range $\sim 0.5 - 1$ TeV with $\mathcal{O}(1)$ values of the parameters g , q , and the hypercharges, for a multiplicity of the gauge fields in the ballpark $N \sim \mathcal{O}(10)$.

Although the aforementioned setup can be generally invoked for a wide range of DM masses (*i.e.* around weak-scale and beyond), we focus in this work on a specific case of how the clockwork mechanism can help realize a weak or near-weak scale CHAMP³, motivated by the following attributes. Firstly, as argued before, this assumes minimalism and thereby avoids large hierarchies with respect to the EW scale. Secondly, a weak-scale CHAMP DM attracts the strongest direct-detection limit on the fractional charge, namely $\epsilon \lesssim 10^{-12}$, which makes it the most interesting minicharged DM candidate to investigate against the role of a clockwork portal in naturally realizing tiny charges. Finally, such a scenario may be testable at some of the upcoming MeV scale gamma-ray telescopes (see *e.g.* ref.[30] for a list of relevant experiments and the corresponding projections).

The paper is structured as follows. Section (2) describes the model in detail. In section (3), we discuss the various theoretical and experimental constraints relevant for the model. Following that, we illustrate the viability of a weak-scale CHAMP as a DM candidate in section (4) for a few representative benchmark configurations. We finally summarize and conclude in section (5).

2 Model

As described above, our goal is to dynamically generate a tiny electrical charge for the DM particle. Since $SU(2)$ charges are necessarily quantized, such a small charge can come about only by generating a minuscule hypercharge for a $SU(2)$ -singlet DM particle. To this end, we begin by constructing a clockwork sector that would serve to extend the hypercharge symmetry of the SM. The next step would be to connect the standard electroweak sector and the clockwork sector, taking care that the thus enhanced model is consistent with all low-energy constraints. Finally, we bring in the dark matter candidate, thereby completing the model. In the following, we delineate each component individually.

2.1 Clockwork with vector fields

Following the treatment in ref.[28], we define the clockwork sector of the model with a gauge symmetry $U(1)^{N+1}$ — each factor corresponding to a gauge field X_μ^j which is spontaneously

³Note that this is markedly different from an interesting DM scenario discussed in ref.[29] where the zero mode of the gauged clockwork sector is a *dark* photon. In that case, it is the SM fermions that are millicharged under the residual dark $U(1)'$ symmetry and the DM remains electrically neutral (*i.e.* with no couplings with the SM photon).

broken, at a characteristic scale⁴ f , to a single $U(1)$ by a configuration of N complex scalars Φ_j . Responsible for the *clockworking* among the gauge fields, this configuration is defined so as to have each scalar Φ_j charged under two adjacent gauge groups, *viz.* $U(1)_j \times U(1)_{j+1}$, with the quantum numbers $(1, -q)$, where $q \gtrsim 1$. The pertinent Lagrangian can be expressed as⁵

$$\mathcal{L}_{CW} = - \sum_{j=0}^N \frac{1}{4} X_{\mu\nu}^j X^{j\mu\nu} + \sum_{j=0}^{N-1} \left[(D_\mu \Phi_j)^\dagger (D_\mu \Phi_j) - \xi \left(\Phi_j^\dagger \Phi_j - \frac{f^2}{2} \right)^2 \right], \quad (2.1)$$

where $X_{\mu\nu}^j$ denote the gauge field strengths and ξ is a dimensionless positive coupling. The covariant derivatives of the scalars are given by

$$D_\mu \Phi_j \equiv [\partial_\mu + ig_x (X_\mu^j - q X_\mu^{j+1})] \Phi_j,$$

where, for the sake of simplicity, we have assumed a universal⁶ gauge coupling g_x across all the $U(1)$ s. Note that the structure of the Lagrangian is reminiscent of moose or quiver theories [31–35], where the individual $U(1)$ ’s can be regarded as *sites* and the complex scalars as the conjoining *link* fields.

The scalar potential in Eq. (2.1) implies that each of the N Φ_j ’s receives a nonzero vacuum expectation value (VEV) given by

$$\langle \Phi_j^\dagger \Phi_j \rangle = \frac{f^2}{2} \quad (2.2)$$

which spontaneously breaks the full gauge symmetry in the pattern $U(1)^{N+1} \rightarrow U(1)_{CW}$, where the conserved charge is given by⁷

$$Q_{CW} = \sum_{j=0}^N q^{-j} Q_j, \quad (2.3)$$

⁴In principle, unequal SSB scales f_i could be accommodated, but only at the cost of introducing additional algebraic complexity without altering the essentials. Large hierarchies between the f_i would, however, negate the spirit of the clockwork paradigm. To avoid such mundane complications, we choose $f_i = f, \forall i$.

⁵With fields carrying nonzero charges under more than one $U(1)$ groups, kinetic mixings between the corresponding gauge bosons are expected to be generated through quantum corrections. In the present case, we only have a single scalar shared between two adjacent groups. Working in the unitary gauge, it is easy to see that the only relevant vertex is the four-point (two scalars and two gauge bosons) one, and the consequent diagrams do not contribute to the gauge-field wave-function renormalization and, hence, to kinetic mixing. The corrections to the masses of the heavy gauge bosons and their mixings are too small to be of any phenomenological consequence.

⁶Eschewing this assumption does not alter the symmetry properties of theory. It will, in general, affect the masses of the gauge fields and their effective couplings with the SM fermions and the dark matter candidate, as will be evident shortly. However, in the absence of large *ad hoc* hierarchies in the gauge couplings, the qualitative features of the model’s phenomenology are adequately addressed with the uniform parametrization.

⁷Had we considered nonuniform gauge couplings g_i , the expression for Q_{CW} would have changed, picking up factors of g_i , but the core essence of the mechanism would have remained unaltered.

with Q_j denoting the individual $U(1)$ generators. Consequently, a total of N gauge fields are Higgsed and receive masses while one combination remains massless, corresponding to the unbroken symmetry $U(1)_{CW}$. The resulting spectrum of the gauge fields is then easily obtained by considering the gauge Lagrangian in the unitary gauge, *i.e.*

$$\mathcal{L}_{gauge}^{(2)} = - \sum_{j=0}^N \frac{1}{4} X_{\mu\nu}^j X^{j\mu\nu} + \sum_{j=0}^N \frac{1}{2} \tilde{M}_{jk}^2 X_{\mu}^j X^{k\mu} , \quad (2.4)$$

where the mass matrix is given by

$$\tilde{M}^2 = g_x^2 f^2 \begin{pmatrix} 1 & -q & 0 & \cdots & 0 \\ -q & 1+q^2 & -q & \cdots & 0 \\ 0 & -q & 1+q^2 & \cdots & 0 \\ \vdots & \vdots & \vdots & \ddots & \vdots \\ 0 & 0 & 0 & \cdots & 1+q^2 \\ & & & & -q \\ 0 & 0 & 0 & \cdots & q^2 \end{pmatrix} . \quad (2.5)$$

Diagonalizing \tilde{M}^2 yields the physical spectrum, namely

$$m_0 = 0 \quad \text{and} \quad m_k^2 \equiv g_x^2 f^2 \lambda_k = g_x^2 f^2 \left(1 + q^2 - 2 q \cos \frac{k\pi}{N+1} \right) \quad (k = 1 \dots N) . \quad (2.6)$$

There is, thus, a mass gap of $\mathcal{O}(g_x f)$ with the heavier states being bunched relatively close. With q being a real number, the transformation between the gauge (X_{μ}) and the mass basis (B_{μ}^0) is simply realized by an orthogonal transformation,

$$X_j^{\mu} = \sum_{k=0}^N O_{jk} B_k^{\mu} \quad (2.7)$$

where the matrix O is specified as

$$O_{j0} = \frac{\mathcal{N}_0}{q^j} , \quad O_{jk} = \mathcal{N}_k \left[q \sin \frac{jk\pi}{N+1} - \sin \frac{(j+1)k\pi}{N+1} \right] , \quad j = 0, \dots, N; \quad k = 1, \dots, N \quad (2.8)$$

with

$$\mathcal{N}_0 \equiv \sqrt{\frac{q^2 - 1}{q^2 - q^{-2N}}} , \quad \mathcal{N}_k \equiv \sqrt{\frac{2}{(N+1)\lambda_k}} .$$

For $q > 1$, the massless state, B_{μ}^0 , is clearly localized towards the 0-th site, *i.e.* has the maximum ($\sim \mathcal{O}(1)$) overlap with X_0^{μ} . Moreover, for sufficiently large N , it has only an exponentially suppressed overlap of magnitude $\sim q^{-N}$ with X_N^{μ} . Thus, a field external to the clockwork sector and charged only under $U(1)_N$ will have but a tiny coupling proportional to q^{-N} with the zero mode B_{μ}^0 , effectively constituting a small charge under $U(1)_{CW}$. We will, subsequently, make use of this feature to naturally generate a very tiny electric charge

Particles	$SU(2)_l$	$SU(3)_c$	$U(1)_0$	$U(1)_1$...	$U(1)_j$	$U(1)_{j+1}$...	$U(1)_N$
ψ_L	2	1	1/2	0	...	0	0	...	0
l_r	1	1	-1	0	...	0	0	...	0
Q_l	2	3	1/6	0	...	0	0	...	0
u_r	1	3	2/3	0	...	0	0	...	0
d_r	1	3	-1/3	0	...	0	0	...	0
H	2	1	1/2	0	...	0	0	...	0
χ	1	1	0	0	...	0	0	...	Y_χ
Φ_j	1	1	0	0	...	1	- q	...	0

Table 1: Charge assignment under extended EW + CW sector scenario.

for the dark matter candidate while assuming all the coupling parameters of the model to be at the $\mathcal{O}(1)$ level⁸.

2.2 The clockwork extended SM

From the preceding discussion, it is clear that a small electric charge for a $SU(2)$ -singlet field localized at the N -th site of the clockwork lattice can be naturally generated if the (conserved) CW symmetry could be identified with the hypercharge component of the SM, *viz.* $U(1)_{CW} \equiv U(1)_Y$. The small overlap of the B_μ^0 with the X_μ^N would then translate to an effectively tiny hypercharge quantum number for such a field (without the need to introduce a hierarchically small quantum number). In doing this, it must be ensured, though, that the construction does not run afoul of low-energy phenomenology, in particular the electroweak precision tests. This is carried out systematically as follows.

We start by assuming the full (**EW + CW**) symmetry of the model Lagrangian to be $SU(2)_L \times U(1)^{N+1}$ with the corresponding charge assignments of the SM fields as listed in Table (1). Thus, in addition to the usual $SU(2)_L$ charges, the SM matter fields (including the Higgs field) are charged under $U(1)_0$, or in other words, are localized at the 0-th site of the CW lattice. Note that the $U(1)_0$ charges for the SM fields are exactly the same as the $U(1)_Y$ charges in the SM. To specify the model completely, we also introduce at this point an extra Dirac fermion χ (as the CHAMP DM candidate) localized at the N -th site. The dynamics and viability of χ as the DM candidate will be thoroughly discussed in a later section. With these definitions, the electroweak Lagrangian in the unbroken phase can be written as

$$\mathcal{L} = \mathcal{L}_{Vis.} + \mathcal{L}_{CW} + \mathcal{L}_{H\Phi} + \mathcal{L}_\chi, \quad (2.9)$$

where $\mathcal{L}_{Vis.}$ defines the gauge-invariant Lagrangian for the SM fermions and the Higgs field H . On the other hand, the component $\mathcal{L}_{H\Phi}$ specifies the mixing between the Higgs and

⁸While the possibility of deriving tiny electromagnetic charges through the clockwork mechanism was hinted at in ref.[28], our model is the first explicit realization of the idea.

the CW scalars, and \mathcal{L}_χ defines the dark sector viz.,

$$\mathcal{L}_{H\Phi} \equiv -\eta \sum_{j=0}^{N-1} H^\dagger H \Phi_j^\dagger \Phi_j \quad \text{and} \quad \mathcal{L}_\chi \equiv \bar{\chi} (i\cancel{D} - m_\chi) \chi . \quad (2.10)$$

In the preceding, η is a real dimensionless coupling⁹, m_χ denotes the mass of the CHAMP and the covariant derivative \mathcal{D} is given by

$$\mathcal{D}_\mu \chi = (\partial_\mu + ig_x Y_\chi X_\mu^N) \chi , \quad (2.11)$$

where the charge Y_χ is presumably $\mathcal{O}(1)$.

On both the CW scalars and the Higgs field acquiring nonzero VEVs (at scales f and v respectively), the symmetry of the theory spontaneously breaks down to a single Abelian factor which is to be identified with the electromagnetic symmetry, *i.e.* $SU(2)_L \times U(1)^{N+1} \rightarrow U(1)_{EM}$. Of course, the minimum of the full (H, Φ) potential depends on the configuration of its parameters, the details of which we defer to a later section. For now, we concentrate only on the gauge sector. The tree-level mass of the W^\pm boson is unaffected by the Abelian sector and, hence, can be ignored in the discussion to follow. On the other hand, in the broken phase, the terms quadratic in the fields W_μ^3 and X_j^μ define a mass matrix given by

$$\mathcal{M}_V^2 = g_x^2 f^2 \begin{pmatrix} \frac{\delta}{4} b^2 & \frac{\delta}{4} b & 0 & 0 & 0 & \dots & \dots & 0 & 0 \\ \frac{\delta}{4} b & 1 + \frac{\delta}{4} & -q & 0 & 0 & \dots & \dots & 0 & 0 \\ 0 & -q & 1 + q^2 & -q & 0 & \dots & \dots & 0 & 0 \\ 0 & 0 & -q & 1 + q^2 & -q & \ddots & \ddots & \vdots & \vdots \\ \vdots & \vdots & \vdots & \vdots & \vdots & \ddots & \ddots & \vdots & \vdots \\ 0 & 0 & 0 & 0 & \dots & \dots & 1 + q^2 & -q & 0 \\ 0 & 0 & 0 & 0 & \dots & \dots & -q & 1 + q^2 & -q \\ 0 & 0 & 0 & 0 & \dots & \dots & 0 & -q & q^2 \end{pmatrix}_{(N+2) \times (N+2)} \quad (2.12)$$

with

$$\delta \equiv \frac{v^2}{f^2} , \quad b \equiv -\frac{g_w}{g_x} .$$

Here, g_w is the $SU(2)_L$ gauge coupling. It can be ascertained easily that \mathcal{M}_V^2 has one zero eigenvalue. As for the other eigenvalues, closed-form analytical expressions are not straightforward for the generic case. However, the task becomes reasonably simple for $v \ll f$ in which case the terms in \mathcal{M}_V^2 proportional to δ can be regarded as perturbations around the CW matrix \tilde{M}^2 . In fact, from a symmetry-breaking perspective, the condition $v \ll f$ can be naively understood as a decoupling of the two SSB scales and, hence, the entire dynamics can be interpreted as a two-step process (see Fig. (1) for an illustration), namely,

$$SU(2)_L \times U(1)^{N+1} \xrightarrow{f} SU(2)_L \times U(1)_{CW} \xrightarrow{v} U(1)_{EM} . \quad (2.13)$$

⁹We could, of course, have introduced nonuniform couplings η_j . This, however, would have only resulted in algebraic complexity without affecting the essential features of the scenario.

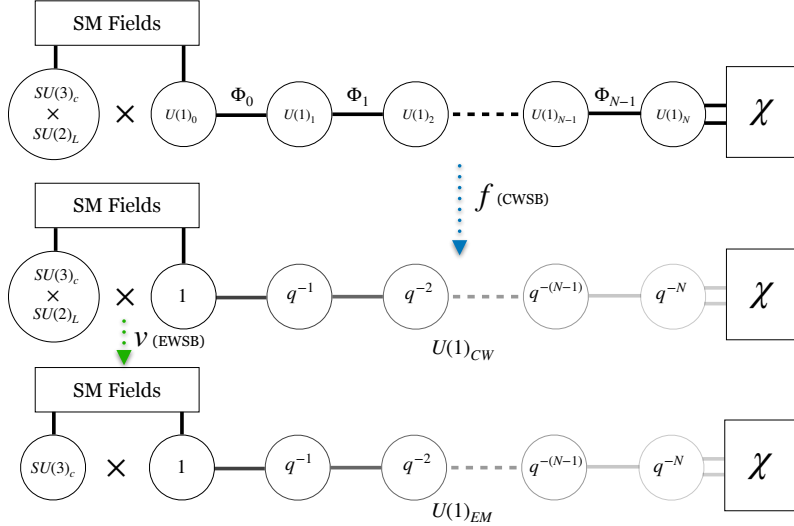


Figure 1: A schematic representation of the two-step symmetry breaking pattern in the model. The first row represents the extended hypercharge construction. In the second row, the individual blobs indicate the exponentially falling (site-dependent) charge under $U(1)_{CW}$. Similarly, in the third row, this translates into the strength of the photon couplings following EWSB (*sans* the overall gauge couplings).

After the first SSB occurs at the scale f , the light gauge boson spectrum in the theory consists of the zeroth CW mode B_μ^0 and the weak bosons W_μ^a , all exactly massless. At this stage, the field B_μ^0 mimics the role of the SM $U(1)_Y$ boson. Understandably, then, one retrieves the usual dynamics of the EW sector after the second SSB at the scale v , albeit with small modulations induced by the CW extension. That there indeed exists a region in the parameter space where deviations as such fall within the known uncertainties in the couplings and masses of the EW gauge bosons will be shown in the next section. For now, we delineate the details of the mass eigenvalues.

Post EWSB, the quadratic terms involving the full set of neutral gauge bosons (in the $W^3 - B^k$ basis) are given by

$$\mathcal{L}_{neut.}^{(2)} \supset \frac{v^2}{8} \left(-gW_\mu^3 + g' \sum_{j=0}^N O_{0j} B_\mu^j \right)^2 + (\text{CW mass terms}). \quad (2.14)$$

where the matrix elements O_{0j} are as given in Eq. (2.8). It is convenient to first identify the photon (A_μ) through a rotation in the (W^3, B^0) plane which reads

$$A_\mu \equiv \sin \theta_W W_\mu^3 + \cos \theta_W B_\mu^0, \quad \text{and} \quad \tilde{Z}_\mu \equiv \cos \theta_W W_\mu^3 - \sin \theta_W B_\mu^0, \quad (2.15)$$

The angle θ_W , quite clearly, acts as an analogue of the Weinberg angle in the SM, and is defined here as $\tan \theta_W = (g_x O_{00}/g_w)$. In terms of the rotated fields, the mass-squared matrix can be written as

$$\tilde{\mathcal{M}}_V^2 \equiv U^T \mathcal{M}_V^2 U \quad (2.16)$$

where the transformation matrix U is defined as

$$\begin{pmatrix} W_\mu^3 \\ X_\mu^0 \\ X_\mu^1 \\ \vdots \\ X_\mu^N \end{pmatrix} = \begin{pmatrix} \cos \theta_W & \sin \theta_W & 0 & \cdots & 0 \\ -\sin \theta_W O_{00} & \cos \theta_W O_{00} & O_{01} & \cdots & O_{0N} \\ -\sin \theta_W O_{10} & \cos \theta_W O_{10} & O_{11} & \cdots & O_{1N} \\ \vdots & \vdots & \vdots & \ddots & \vdots \\ -\sin \theta_W O_{N0} & \cos \theta_W O_{N0} & O_{N1} & \cdots & O_{NN} \end{pmatrix} \begin{pmatrix} \tilde{Z}_\mu \\ A_\mu \\ B_\mu^1 \\ \vdots \\ B_\mu^N \end{pmatrix}. \quad (2.17)$$

Given that A_μ is strictly massless, the (nondiagonal) matrix $\tilde{\mathcal{M}}_V^2$ has rank $(N+1)$ and can be trivially reduced to

$$\tilde{\mathcal{M}}_V^2 \rightarrow \begin{bmatrix} m_{\tilde{Z}}^2 & \Delta^T \\ \Delta & \mathcal{M}'^2 \end{bmatrix}_{(N+1) \times (N+1)}. \quad (2.18)$$

Here,

$$m_{\tilde{Z}}^2 \equiv \frac{v^2}{4} (g_x^2 O_{00}^2 + g_w^2), \quad (2.19)$$

alongwith the aforementioned identification $g_Y = g_x O_{00}$, would have denoted the tree-level mass of the SM Z -boson in the absence of mixings with the higher B_k 's ($k, l = 1 \dots N$) as encoded in

$$\begin{aligned} \Delta_k &= -\frac{g_w^2}{4 \cos \theta_W} v^2 O_{0k}, \\ (\mathcal{M}'^2)_{kl} &= g_x^2 f^2 \lambda_k \delta_{kl} + \frac{g_x^2 v^2}{4} O_{0k} O_{0l}. \end{aligned} \quad (2.20)$$

To leading order in v^2/f^2 , the Z boson is, then, identified as

$$Z_\mu \simeq \tilde{Z}_\mu + \frac{v^2 O_{00}}{4 f^2 \sin \theta_W} \sum_{k=1}^N \left(\frac{1}{\lambda_k} \sin \frac{k\pi}{N+1} \right) B_\mu^k + \mathcal{O}\left(\frac{v^4}{f^4}\right) \quad (2.21)$$

and the corresponding mass eigenvalue given by

$$m_Z \simeq m_{\tilde{Z}} \left[1 - \frac{v^2}{4 f^2 (N+1)} \sum_{k=1}^N \frac{1}{\lambda_k^2} \sin^2 \frac{k\pi}{N+1} \right] + \mathcal{O}\left(\frac{v^4}{f^4}\right). \quad (2.22)$$

While the obtained deviations from the SM expectations are crucial for the Z boson, as discussed in the next section, the corresponding corrections for the heavier gauge bosons can safely be neglected, and the corresponding physical states along with their masses can be well approximated as

$$Z_\mu'^k \simeq B_\mu^k, \quad m_k \simeq g_x f \sqrt{\lambda_k}. \quad (2.23)$$

With the above identification, the couplings of the neutral gauge bosons to the SM currents J_{SM}^f (for a given fermion f), as well as to the dark matter particle χ , can be parametrized in terms of vector and axial-vector couplings $g_{V/A}^{f,i}$

$$\begin{aligned} g_{V/A}^{f,i} &= \frac{1}{2} \left(g_x U_{1i} (Y_L^f \pm Y_R^f) + g_w U_{0i} T^{3,f} \right) \\ g_{V/A}^{\chi,i} &= g_x U_{Ni} Y_\chi, \end{aligned} \quad (2.24)$$

where we have omitted the higher order corrections in v^2/f^2 .

Contrary to the usual convention of labeling a multi-field spectrum according to the hierarchy in masses, we choose to label the lightest modes, *i.e.* the photon and the Z boson, according to their overlaps with the *pure* SM vector fields in their gauge basis—in our context this happens to be the W^3 field. With this prescription, therefore, the zeroth mode corresponds to the Z boson while the first mode corresponds to the photon, and the heavier Z'_k modes are then labeled according to their masses. Thus, for any fermion f , Eq. (2.24) gives

$$g_V^{f,1} = eQ_f \quad ; \quad g_A^{f,1} = 0 \quad (2.25)$$

where $Q_f = Y_L^f + T^{3,f} = Y_R^f$ denotes the electromagnetic charge of the fermion f . Similarly, the $\gamma W^+ W^-$ coupling too remains unaltered, while for DM, the electromagnetic coupling is given by

$$g^{\chi,1} = Y_\chi q^{-N} e \equiv \epsilon e . \quad (2.26)$$

For the Z boson (corresponding to the index “0” in Eq. (2.24)), the tree-level vector and axial-vector couplings are given by

$$\begin{aligned} g_V^{f,0} &= \frac{g_w}{\cos \theta_W} \left[\left(T^{3,f} - 2Q_f \sin^2 \theta_W \right) + \delta g_V^{f,0} \right], \\ g_A^{f,0} &= \frac{g_w}{\cos \theta_W} \left[T^{3,f} + \delta g_A^{f,0} \right]. \end{aligned} \quad (2.27)$$

The first terms on the right-hand side of Eq. (2.27) correspond to the leading-order SM couplings obtained from Eq. (2.24), while $\delta g_{V/A}^{f,0}$ denote the corrections induced by the CW sector, and are given by

$$\delta g_{V/A}^{f,0} = -\frac{v^2}{4f^2} \frac{(Y_L^f \pm Y_R^f)}{(N+1)} \sum_{k=1}^N \frac{1}{\lambda_k^2} \sin^2 \frac{k\pi}{N+1} . \quad (2.28)$$

As before, we neglect variations in the effective couplings of the heavier CW gauge bosons to the SM sector, since these effects are strongly suppressed and do not lead to qualitative changes in the phenomenology.

3 Constraints

While our model does have many fields beyond the SM, it is quite economic in terms of the new parameters, having only seven additional ones. These include the clockwork factor q , which controls the exponential localization of modes across the clockwork sites and, thereby, determines the apparently hierarchical structure of couplings; the number of vector clockwork sites N , which governs the resolution and extent of the clockwork chain; and the clockwork symmetry breaking (CWSB) scale f , which sets the mass scale of the heavy states arising from the clockwork sector.

Additionally, the quartic coupling ξ describes self-interactions within the heavy scalar sector, whereas the coupling η dictates the interaction strength between the Standard Model

Higgs and the clockwork scalars, leading to mixing between them¹⁰. Finally, the dark matter sector itself is characterised by two parameters, the mass m_χ and Y_χ , its charge under the extremal $U(1)$.

As with any model going beyond the SM, the new fields and parameters are subject to both experimental as well as theoretical constraints and it is useful to discuss these individually.

3.1 Theoretical constraints

The theoretical constraints, as can be imagined, arise primarily in the context of the high-energy behaviour of the multi-scalar potential which, in turn, crucially dictates the validity of the clockwork mechanism in the far UV. In the following, therefore, we delineate the various elements of the scalar sector in the model and assess the stability of the configuration under renormalization group (RG) evolution.

The full scalar potential of the theory reads

$$V(H, \{\Phi_j\}) = \lambda \left(H^\dagger H - \frac{v^2}{2} \right)^2 + \xi \sum_{j=0}^{N-1} \left(\Phi_j^\dagger \Phi_j - \frac{f^2}{2} \right)^2 + \eta H^\dagger H \sum_{j=0}^{N-1} \Phi_j^\dagger \Phi_j, \quad (3.1)$$

and for it to be bounded from below, one needs

$$\lambda, \xi > 0 \quad \text{and} \quad N\eta^2 < 4\lambda\xi. \quad (3.2)$$

The last-mentioned is an important constraint as would, shortly, be evinced below.

In the unitary gauge, the fields may be expressed in terms of the vacuum expectation values v and f as

$$H = \begin{pmatrix} 0 \\ \frac{\tilde{h}+v}{\sqrt{2}} \end{pmatrix}, \quad \Phi_j = \frac{\tilde{\phi}_j + f}{\sqrt{2}}. \quad (3.3)$$

Clearly, the field \tilde{h} mixes only with one specific combination of the $\tilde{\phi}_j$, namely

$$\tilde{\Phi} = \frac{1}{\sqrt{N}}(\tilde{\phi}_0 + \tilde{\phi}_1 + \cdots + \tilde{\phi}_{N-1}). \quad (3.4)$$

Consequently, the matrix is trivially diagonalized with the eigenvalues given by

$$\begin{aligned} m_h^2 &= \lambda v^2 + \xi f^2 - \sqrt{(\xi f^2 - \lambda v^2)^2 + \frac{N}{4}\eta^2 f^2 v^2}, \\ m_\Phi^2 &= \lambda v^2 + \xi f^2 + \sqrt{(\xi f^2 - \lambda v^2)^2 + \frac{N}{4}\eta^2 f^2 v^2}, \\ m_{\varphi_k}^2 &= 2\xi f^2 \quad (k = 1, \dots, N-1). \end{aligned} \quad (3.5)$$

where φ_k are orthogonal to $\tilde{\Phi}$ and to each other. A simple identification would be with the diagonal generators of $SU(N)$, but with these states being degenerate, any linear combination is as good. As the expressions for φ_k s are not relevant for our analysis, we shall

¹⁰Note that the gauge coupling g_x is not a new parameter, having replaced the usual hypercharge coupling in the SM.

consider these no further. The remaining two mass eigenstates h and Φ are easily identified to be

$$\begin{pmatrix} h \\ \Phi \end{pmatrix} = \begin{pmatrix} \cos \zeta & -\sin \zeta \\ \sin \zeta & \cos \zeta \end{pmatrix} \begin{pmatrix} \tilde{h} \\ \tilde{\Phi} \end{pmatrix} \quad (3.6)$$

with the mixing angle ζ being given by

$$\tan 2\zeta = \frac{\sqrt{N} \eta f v}{2(\xi f^2 - \lambda v^2)}. \quad (3.7)$$

In the limit of $v \rightarrow 0$, not only does the mixing disappear, but Φ becomes degenerate with the φ_k , as it should. This is only a reflection of the $SU(N)$ symmetry in the pure Φ_j sector, broken only by the other interactions.

Note that the aforementioned bound on $N\eta^2$ Eq. (3.2) not only serves to keep m_h^2 positive—see the first of Eqs.(3.5)—but also controls the Higgs mixing angle, which cannot be too large. In addition, the stability condition must hold true at least upto a putative UV cutoff scale as the parameters of the potential undergo RG evolution. Understandably, this places the strongest theoretical upper bound on η in the IR (*i.e.* around the scale f).

The aforementioned constraints have been imposed only on the tree-level parameters. One must also ensure not only that the couplings do not become nonperturbative under RG evolution but also that the stability of the potential is not compromised until a cutoff scale $\Lambda \gg f$. Limiting ourselves to only a one-loop analysis, we have

$$\begin{aligned} 16\pi^2\beta_\lambda &\approx \frac{3}{8}g_x^4 + \frac{3}{4}g_x^2g_w^2 + \frac{9}{8}g_w^4 - 3g_x^2\lambda - 9g_w^2\lambda + 24\lambda^2 + N\eta^2 + 12y_t^2 - 6y_t^4 \\ 16\pi^2\beta_\xi &\approx 6g_x^4(1+q^2)^2 - 12g_x^2(1+q^2)\xi + 2\eta^2 + 20\xi^2 \\ 16\pi^2\beta_\eta &\approx 3g_x^4 + 4\eta^2 + \eta \left(-\frac{15}{2}g_x^2 - \frac{9}{2}g_w^2 + 12\lambda + 8\xi - 6g_x^2q^2 + 6y_t^2 \right) \end{aligned} \quad (3.8)$$

Here $\beta_p \equiv dp/dt$, with $t = \ln(\mu/\mu_0)$, where μ is with μ being the renormalisation scale and $\mu_0 = m_t$ the reference scale at which the boundary conditions are defined. While the evolutions of the nonabelian gauge couplings remain unaltered, that for the $U(1)$ factors is more nuanced. For $k = 1 \dots (N-1)$, the gauge boson X_k couples only to the scalars Φ_{k-1} and Φ_k carrying charges $-q$ and 1 respectively. With the scalars having equal masses, the corresponding gauge couplings evolve identically. The story for $U(1)_0$ and $U(1)_N$ is different. The first couples to all of the SM fermions, the Higgs field H as well as the scalar Φ_0 . Hence, the evolution of this coupling is very similar to that for the $U(1)_Y$ inside the SM. The $U(1)_N$, on the other hand, couples to only Φ_{N-1} (with a charge $-q$) and the DM χ (with a charge Y_χ), and so its coupling evolves differently from all others. This, of course, brings into question our simplifying assumption of all the $U(1)$ field having identical coupling constants. However, given that the evolutions are slow and the cutoff Λ for the theory not too large (see the next subsection), if the couplings at the scale Λ are held identical, $g_x(0)$ and $g_x(N)$ would differ from the rest only minimally. As we have argued earlier, the consequent changes in the phenomenology would be only quantitative, and that too minimal.

The evolution of λ receives a positive contribution from the Higgs-CW sector interaction through the $N\eta^2$ term. For large N or sizable coupling η , this contribution can enhance the running of λ , thereby partially compensating for the destabilising effect induced by the top Yukawa coupling. On the other hand, too large a value for $N\eta^2$ would, nominally, tend to render λ nonperturbative. Fortunately, the value of $N\eta^2(t = 0)$ required to do this is too large to be of phenomenological interest. Consequently, the overall behaviour of λ depends sensitively on the chosen benchmark parameters.

The evolution of the CW-sector self-coupling ξ is dominantly driven by gauge interactions through the term proportional to $g_x^4(1 + q^2)^2$, reflecting its strong sensitivity to the parameter q . In addition, the positive self-interaction contribution $20\xi^2$ leads to a rapid growth of ξ at high scales, potentially driving it towards a Landau pole for sufficiently large initial values. The term proportional to η^2 remains subdominant for $\eta < \xi$, which is natural choice considering in view of the stability condition of (3.2).

Finally, the running of the Higgs-CW coupling η is governed by a balance between scalar and gauge effects. Positive contributions arise from scalar self-interactions (involving the parameters λ , ξ , and η), as well as from the top Yukawa coupling y_t , whereas gauge interactions induce negative contributions. In particular, the term proportional to ξ becomes dominant and leads to an accelerated enhancement of η in the ultraviolet. For moderate starting values of $N\eta^2$ and ξ , the change in η is confined to a few percent for a cutoff $\Lambda \sim 10^3$ TeV. Given this, it is easy to see that the conditions of $\xi > 0$ is never violated and even $N\eta^2 < 4\lambda\xi$ is not violated until one almost hits the epoch of metastability of the SM Higgs (which, as we have argued above, is postponed compared to the case of the SM).

In summary, while the couplings η and ξ are simultaneously constrained by Higgs–scalar mixing limits, vacuum stability, and triviality requirements, the restrictions are not too severe. With $\lambda \simeq 0.12$, $v \simeq 246$ GeV being given, and even allowing for a maximal Higgs mixing with a singlet scalar *viz.* $\sin\zeta \lesssim 0.1$ [36], Eq. (3.7) implies $\eta \lesssim 0.1$ for $\xi \simeq 0.7$, assuming $f \simeq 1$ TeV and $N = 20$. This constraint is further relaxed for larger values of f , while the RG evolution governed by Eq. (3.8) remains perturbative and safely below the triviality bound up to scales of at least 10^3 TeV.

3.2 Experimental constraints

Confronting the parameter space of our model with experimental data, the most stringent constraints emanate from sources like electroweak precision measurements, collider searches (especially in the dilepton channel), and direct detection experiments targeting dark matter. Electroweak observables, measured with high accuracy at colliders, are particularly sensitive to new physics that modifies the gauge boson sector as well as the scalar sector, while direct detection bounds constrain the allowed strength and structure of interactions between the DM and the SM particles.

3.2.1 Electroweak Constraints

First and foremost, note that g_w —the $SU(2)_L$ gauge coupling—remains the same as in the SM; and while M_W may receive small radiative corrections from the clockwork Z' bosons, such corrections would turn out to be negligible due to the suppressed coupling of W^3 to

the heavy clockwork states, and can be safely ignored. Thus we may safely retain the SM relation

$$g_w^2 = \frac{8G_F M_W^2}{\sqrt{2}}. \quad (3.9)$$

Further, the identification of g_Y elucidated in the preceding section, *viz.*

$$g_x O_{00} = g_x \sqrt{\frac{q^2 - 1}{q^2 - q^{-2N}}} \equiv g_Y = \frac{e}{\cos \theta_W}, \quad (3.10)$$

implies a relation between the parameters g_x , q , and N . The relation above could also be rewritten as

$$e = \frac{g_x g_w O_{00}}{\sqrt{g_x^2 O_{00}^2 + g_w^2}}. \quad (3.11)$$

Reminding ourselves that the DM coupling to the photon—given by $g^{\chi,1} = eq^{-N} Y_\chi$ —has to be tiny, q^N needs to be very large unless Y_χ is unnaturally small. This, in turn, means that N essentially decouples from the relation in Eq. (3.10) and $O_{00} \simeq \sqrt{1 - q^{-2}}$. In other words, the fine structure constant essentially imposes a relation between g_x and q , almost independent of the other parameters in the theory.

At this stage, we are in a position to examine the electroweak precision observables. As shown above, both the mass and the couplings of the Z boson receive tree-level modifications from the CW sector, as given in Eqs. (2.22) and (2.28), respectively. We now move to the well-known electroweak precision observables, and begin by discussing the shift in the Z -boson mass, which can be expressed in terms of the oblique parameter T , defined as

$$T = \frac{-1}{\alpha} \frac{\Pi_{ZZ}^{\text{new}}(0)}{m_Z^2}. \quad (3.12)$$

Here, α is the electromagnetic coupling evaluated at the Z pole, and $\Pi_{ZZ}^{\text{new}}(0) = m_Z^2 - (m_Z)^2$. Since no tree-level corrections accrue to the W -boson mass, the T parameter, in our setup, can be split neatly into the tree-level contribution from the correction to the Z -boson mass and the usual one-loop corrections within the SM. In this, we are neglecting the quantum corrections accruing from the new physics particles in the loops, as these are too small to be of any consequence. We then have,

$$\alpha T_{\text{tree}} = \frac{v^2}{2f^2(N+1)} \sum_{k=1}^N \frac{1}{\lambda_k^2} \sin^2 \frac{k\pi}{N+1}, \quad (3.13)$$

whereas the expression for T_{SM} remains unchanged. T_{tree} has the most pronounced dependence on the parameter q and f , and, in Fig. (2), we display the resulting exclusion regions for a fixed N .

Of equal importance are the Z -couplings to the SM fermions. Within the SM, the *observable* Weinberg angle $\tilde{\theta}_W$ is expressed in terms of the parameter appearing in the Lagrangian through [37]

$$\sin^2 \tilde{\theta}_W \cos^2 \tilde{\theta}_W = \sin^2 \theta_W \cos^2 \theta_W (1 + \alpha T_{\text{tree}}). \quad (3.14)$$

The effective couplings corresponding to the tree-level ones—see Eq. (2.27)—can, then, be parametrized as

$$\tilde{g}_V^{f,0} = \frac{e}{\sin \tilde{\theta}_W \cos \tilde{\theta}_W} \left(\tilde{g}_{V,\text{SM}}^{f,0} + \delta \tilde{g}_V^{f,0} \right), \quad (3.15)$$

$$\tilde{g}_A^{f,0} = \frac{e}{\sin \tilde{\theta}_W \cos \tilde{\theta}_W} \left(\tilde{g}_{A,\text{SM}}^{f,0} + \delta \tilde{g}_A^{f,0} \right). \quad (3.16)$$

where $\tilde{g}_{V,\text{SM}}^{f,0} = T^{3,f} - 2Q_f \sin^2 \tilde{\theta}_W$ and $\tilde{g}_{A,\text{SM}}^{f,0} = T^{3,f}$ denote the SM contributions to the vector and axial-vector couplings, respectively. The deviations $\delta \tilde{g}_{V,A}^{f,0}$ encode the effects of new physics and are given as

$$\delta \tilde{g}_V^{f,0} = \frac{1}{2} \alpha T_{\text{tree}} \left(\tilde{g}_{V,\text{SM}}^{f,0} + Q_f \frac{\sin \tilde{\theta}_W \cos \tilde{\theta}_W}{\cos^2 \tilde{\theta}_W - \sin^2 \tilde{\theta}_W} \right) + \delta g_V^{f,0}, \quad (3.17)$$

$$\delta \tilde{g}_A^{f,0} = \frac{1}{2} \alpha T_{\text{tree}} \left(\tilde{g}_{A,\text{SM}}^{f,0} + Q_f \frac{\sin \tilde{\theta}_W \cos \tilde{\theta}_W}{\cos^2 \tilde{\theta}_W - \sin^2 \tilde{\theta}_W} \right) + \delta g_A^{f,0}, \quad (3.18)$$

with $\delta g_{V/A}^{f,0}$ denoting the tree-level deviations from the SM induced by the new physics, as given in Eq. (2.28).

While a global fit to all electroweak precision data is possible, it suffices to consider the measurements with the highest sensitivities, namely the total decay width of the Z boson, Γ_Z ,

$$\Gamma_Z = \Gamma_Z^{\text{SM}} \left[1 + 2 \sum_f \frac{\tilde{g}_{V,\text{SM}}^{f,0} \delta \tilde{g}_V^{f,0} + \tilde{g}_{A,\text{SM}}^{f,0} \delta \tilde{g}_A^{f,0}}{(\tilde{g}_{V,\text{SM}}^{f,0})^2 + (\tilde{g}_{A,\text{SM}}^{f,0})^2} \right]. \quad (3.19)$$

and the left-right asymmetry A_e as measured by the SLD and LEP,

$$A_e = A_{e,\text{SM}} \left[1 + 4 \frac{(\tilde{g}_{L,\text{SM}}^{e,0})^2 (\tilde{g}_{R,\text{SM}}^{e,0})^2}{(\tilde{g}_{L,\text{SM}}^{e,0})^4 - (\tilde{g}_{A,\text{SM}}^{e,0})^4} \left(\frac{\delta \tilde{g}_L^{e,0}}{g_{L,\text{SM}}^{e,0}} - \frac{\delta \tilde{g}_R^{e,0}}{g_{R,\text{SM}}^{e,0}} \right) \right]. \quad (3.20)$$

with the left- and right-handed couplings obtained from the vector and axial couplings as $\tilde{g}_{L/R}^{e,0} = \tilde{g}_V^{e,0} \pm \tilde{g}_A^{e,0}$. The quantities Γ_Z^{SM} and $A_{e,\text{SM}}$ denote the Standard Model predictions for the Z -boson decay width and the LR asymmetry, respectively, including radiative corrections. The current experimental measurements, $\Gamma_Z^{\text{exp}} = 2.4955 \pm 0.0023$ and $A_e^{\text{exp}}(\text{LEP}) = 0.1498 \pm 0.0049$ [19], are in excellent agreement with the SM results, thereby placing stringent constraints as depicted in Fig. (2). As can be seen, the constraints imposed by the individual EW observables (T , Γ_Z and A_e) on the $(q-f)$ plane are largely similar in effect, with the ones resulting from A_e being slightly weaker. For reference, we also indicate the direct detection bound on q for a fixed N , corresponding to the allowed region for millicharged dark matter, with a red vertical line, which will be discussed in the next section.

As for the parameters of the extended scalar sector, the experimental measurements primarily constrain the $\Phi-h$ mixing angle ζ . These bounds arise from a number of sources, namely the electroweak precision observables; the measured W mass; the observed signal strengths of the 125 GeV Higgs resonance at ATLAS and CMS; as well as limits from

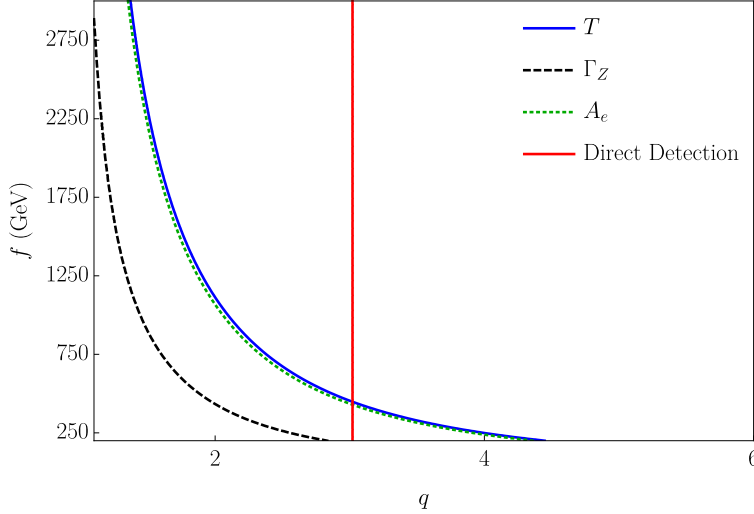


Figure 2: Bounds from Z -pole observables in the (q, f) parameter space for fixed $N = 25$ at the 68% CL. The region to the above each curve is allowed. The black dashed curve corresponds to the constraint from the Z -boson decay width, the blue solid curve arises from the oblique parameter T (we have taken $T = 0.01 \pm 0.12$ [19]), and the green dashed curve represents the constraint from the electron left-right asymmetry. The red vertical line indicates the lower bound on q for the given N , as required by direct detection limits on fractionally charged DM (discussed in the next section).

SM Higgs invisible decays (for light new scalars). Also relevant are constraints from direct searches for new scalar resonances at the LEP, Tevatron, and the LHC. The aforementioned constraints have been thoroughly investigated in the literature [36, 38–41] and are directly applicable to our setup. For the new scalar masses in the range $2m_h \text{ GeV} \lesssim m_\Phi \lesssim 600 \text{ GeV}$, the bounds on $\sin \zeta$ are dominated by those from direct searches for $\Phi \rightarrow ZZ$, $\Phi \rightarrow VV$ and $\Phi \rightarrow hh$, whereas for $m_\Phi \gtrsim 600 \text{ GeV}$ constraints from higher-order contributions to the W mass prevail. In both the cases, though, the upper limit amounts to $|\sin \zeta| \lesssim 0.15$ [41, 42].

Additionally, for the opposite case of $m_h < m_\Phi < 2m_h$, strong constraints on the mixing angle apply from the exclusion limits from Higgs searches at LHC [36], whereas for $m_\Phi < m_h$, the same is constrained by measurements of the Higgs signal strength at LEP [43]. However, given the current experimental lower limits on the Z' masses in our model (to be discussed later), the allowed CWSB scale can be roughly estimated to be $f \gtrsim 1 \text{ TeV}$. Consequently, with the assumption that $\xi \sim \mathcal{O}(1)$, the heavy CW scalars are naturally expected to have commensurate masses, *i.e.* $m_\Phi \gtrsim 1 \text{ TeV}$. With this in mind, we do not explore the case $m_\Phi < 2m_h$ any further.

3.2.2 Direct detection constraints

Direct detection experiments largely employ bolometric devices dependent on energy transferred in the DM particle recoiling off the detector atoms (essentially the nuclei). Consequently, non-detection places upper bounds on the recoil cross sections.

In the present context, this is driven by a series of t -channel diagrams, with the mediators being all the neutral gauge bosons in the theory (the photon, the Z , and all of the Z' s). The amplitude, for scattering off a quark q , can be represented as

$$\mathcal{M} = t^{-1} J_{1\mu}^{(\chi)} J_1^{(q)\mu} + (t - m_Z^2)^{-1} J_{0\mu}^{(\chi)} J_0^{(q)\mu} + \sum_{k=1}^N \left(t - m_{Z'_k}^2 \right)^{-1} J_{k+1,\mu}^{(\chi)} J_{k+1}^{(q)\mu}$$

where the appropriate gauge couplings have been subsumed in the currents. In the above, due to the vector-like coupling of DM to the vector fields, the contributions corresponding to the longitudinal polarization modes of the massive gauge bosons disappear identically. Furthermore, as the momentum exchanged is small (typically in the range of 10–100 MeV for non-relativistic DM), the Mandelstam variable t can safely be neglected in all but the photon diagram. In other words, the amplitude depends on combinations such as

$$-t^{-1} g^{\chi,1} g_V^{q,1} + m_Z^{-2} g^{\chi,0} (g_V^{q,0} + g_A^{q,0} \gamma^5) + \sum_{k=1}^N m_{Z'_k}^{-2} g^{\chi,k+1} (g_V^{q,k+1} + g_A^{q,k+1} \gamma^5), \quad (3.21)$$

where we have used the fact that the DM-current is inherently vectorial.

As we have seen earlier, the DM's couplings to both the photon and the Z are highly (and almost equally) suppressed, while those to the heavier gauge bosons are not. And since $m_Z^2 \gg |t|$, the Z -contribution can be safely neglected, leaving only the photon and the Z' bosons as relevant mediators.

For the case of the vector-like part of the quark current, the combination of Eq. (3.21) can, thus, be approximated by

$$\mathcal{P} \approx \mathcal{P}_\gamma + \sum_{k=1}^N \mathcal{P}_k, \quad (3.22)$$

with

$$\mathcal{P}_\gamma = \frac{e^2 Q_q Y_x}{2 q^N t} \quad (3.23)$$

$$\mathcal{P}_k = \frac{Y_\chi (Y_L^q + Y_R^q)}{N} \frac{q}{f^2} \frac{(-1)^k}{\lambda_k^2} \sin^2 \left(\frac{k \pi}{N+1} \right) \quad (3.24)$$

being the contributions from photon and Z'_k mediation, respectively.

For the axial quark current, the photon term is, of course, absent. The Z' -mediated contributions have the same structure as above, with $(Y_L^q - Y_R^q)$ replacing $(Y_L^q + Y_R^q)$ and, therefore, exhibits the same qualitative behavior as in the case of the vector current.

At this stage, it behoves us to reexamine the case of all the Z 's being infinitely heavy. The amplitude, then, would be dominated by the photonic diagram alone. Since a cryogenic bolometer is sensitive to a small deposition of energy, the detectable recoil cross section can be sufficiently large unless $g^{\chi,0}$ is small enough. This is why the constraint on the charge of the DM is orders of magnitude stronger than what the name “millicharged” conveys. A second important feature, characteristic of the clockwork construction, is manifest in the collective effect of the entire set of Z' bosons. Note that the individual contributions

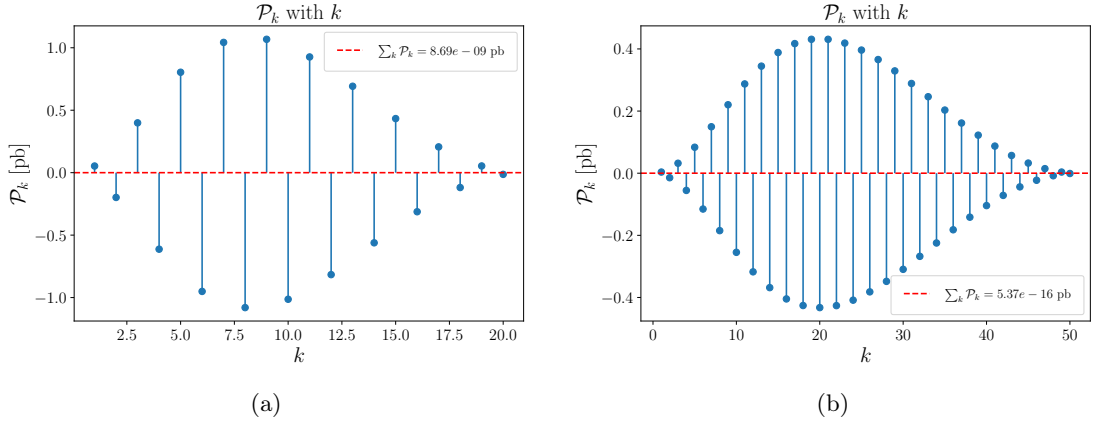


Figure 3: Variation of \mathcal{P}_k for $\chi\bar{\chi} \rightarrow e^-e^+$ (i.e $Y_L = -0.5, Y_R = -1.0$ and taken $Y_\chi = 1.0$), given by (3.24) corresponding to different Z'_k states for $q = 3.0$ and $f = 3000$ GeV, shown for two different cases: (a) $N = 20$ and (b) $N = 50$. The blue dots represent the individual contributions (in picobarns) from each Z'_k , while the red line denotes the summed contribution, which exhibits a pronounced cancellation effect.

alternate in sign, leading to significant cancellations. As a result, the net amplitude is strongly suppressed despite the individual Z' states having $\mathcal{O}(1)$ couplings to DM. This behavior is illustrated in Fig. (3), where the total summed contribution is compared against the individual terms for representative benchmark points. Apart from this, a further global suppression with increasing N is also observed if we compare subplots in Fig. (3), and is consistent with the explicit N^{-1} dependence in Eq. (3.21). If we compare this to the photon contribution, which scales as q^{-N} , we see that, for sufficiently large N , the photon contribution eventually becomes subdominant, despite the collective cancellations among the Z' modes. On the other hand, for moderate values of N —the phenomenologically attractive situation—the photon channel remains dominant by several orders of magnitude, allowing us to safely neglect the Z' contributions in this context.

Having established the relative roles of the photon, Z , and Z' channels, we now turn to the phenomenologically relevant region of the parameter space and the corresponding experimental constraints. Since our focus here is on millicharged dark matter, we first consider the photon-mediated contribution. An estimate of the electromagnetic cross section for dark matter–proton scattering is given by [44]

$$\sigma_p = \frac{16\pi\alpha^2\epsilon^2\mu_{\chi p}^2}{(2m_N E_R)^2}, \quad (3.25)$$

where σ_p denotes the scattering cross section between the proton and the dark matter particle χ . Here α is the fine-structure constant, ϵ is the charge ratio between the dark matter particle and the proton, $\mu_{\chi p}$ is the reduced mass of the proton– χ system, m_N is the nuclear mass of the target, and E_R is the recoil energy imparted during scattering. Since the nucleon charge is simply the sum of the constituent quark charges, the DM–quark interaction

straightforwardly translates to the DM–proton interaction. If the photon is the only mediator between the DM and the visible sector, direct detection bounds constrain the parameters q and N through the relation $\epsilon = Y_\chi q^{-N}$, with Y_χ taken to be an $\mathcal{O}(1)$ quantity. From current direct detection results, the most stringent limits arise from the LUX-ZEPLIN (LZ-2025) experiment[45]. Over a wide range of dark matter masses, extending from $\mathcal{O}(10)$ GeV to the multi-TeV scale, LZ sets upper limits on the spin-independent DM–nucleon scattering cross section at the level of $10^{-12}–10^{-10}$ pb.

Using Eq. (3.25) for a Xenon target, this implies $\epsilon \sim 10^{-12}$ for $\mathcal{O}(1)$ TeV DM. This bound translates into a lower limit on N for a given q . For example, for $q \simeq 3.0$, one requires $N \gtrsim 24$. The most interesting scenarios are, therefore, those with relatively small N , since these lie within the reach of future searches. For $(q \simeq 3.0, N \simeq 25)$, the collective Z' contribution is suppressed by several orders of magnitude compared to the photon channel, and becomes comparable only for $N \sim 30$. Thus, our earlier assumption that the heavy vector contributions can be neglected in such a region remains well justified.

3.2.3 Collider Bounds

At the LHC, the Z'_k may, of course, be produced, at the tree order, from $q\bar{q}$ -fusion. Of the decay modes into the SM particles, the dominant one is into a $q\bar{q}$ pair. However, the QCD backgrounds to dijet production are overwhelmingly large, notwithstanding the existence of resonances. Hence, we turn to the Drell-Yan process, namely $pp \rightarrow \ell^+\ell^-$. The relevant parameter R_k is defined as [46]

$$R_k = \frac{\sigma(pp \rightarrow Z'_k \rightarrow \ell^-\ell^+)}{\sigma(pp \rightarrow Z \rightarrow \ell^-\ell^+)} \xrightarrow{\text{NWA}} \frac{\sigma(pp \rightarrow Z'_k)}{\sigma(pp \rightarrow Z)} \times \frac{\mathcal{BR}(Z' \rightarrow \ell^-\ell^+)}{\mathcal{BR}(Z \rightarrow \ell^-\ell^+)}, \quad (3.26)$$

with the second step holding under the narrow width approximation. The first fraction on the right-hand side (resonant production) can be easily calculated, even incorporating the QCD-corrections as available in the literature [47], or even estimated from existing Z' studies by accordingly scaling with the couplings. As for the second factor (ratio of branching fractions), couplings of a given Z'_k to the SM fermions are proportional to their hypercharges, and thus, $\Gamma(Z'_k \rightarrow \ell^+\ell^-)/\Gamma(Z'_k \rightarrow SM)$ is expected to be approximately SM-like (the opening of the $t\bar{t}$ channel does not significantly alter this ratio). Nonetheless, note that one of the major decay modes of the Z'_k is that in the DM *viz.*, $\chi\bar{\chi}$. However, as it would turn out, the reproduction of the correct relic abundance would stipulate $Y_\chi \lesssim 0.5$ leading to $\text{BR}(Z'_k \rightarrow \chi\bar{\chi}) \lesssim 0.4$. The presence of this additional channel, though, does not render the aforementioned ratio of the branching significantly smaller than order unity.

Going beyond the naive estimates, we present, in Fig. (4), the values of R_k , for a specific benchmark point that would be seen (in next section) to yield the correct relic density, *i.e.* $q = 3$, $N = 25$, $f = 3$ TeV, $Y_\chi = 0.2$. The largest relative signal strength, in this case, occurs for $k = 5$ (with $m_5 \simeq 2564$ GeV). Therefore, a representative lower bound on the SSB scale f can be obtained by comparing the relative signal strengths in the model with the corresponding experimental limits from dilepton searches [46, 48] for varying masses of Z'_5 . This is carried out in Fig. (5) for $q = 3, 4$, which translates into the lower bounds $f \gtrsim 2$ TeV and $f \gtrsim 1$ TeV, respectively. Although the aforementioned limits have been derived

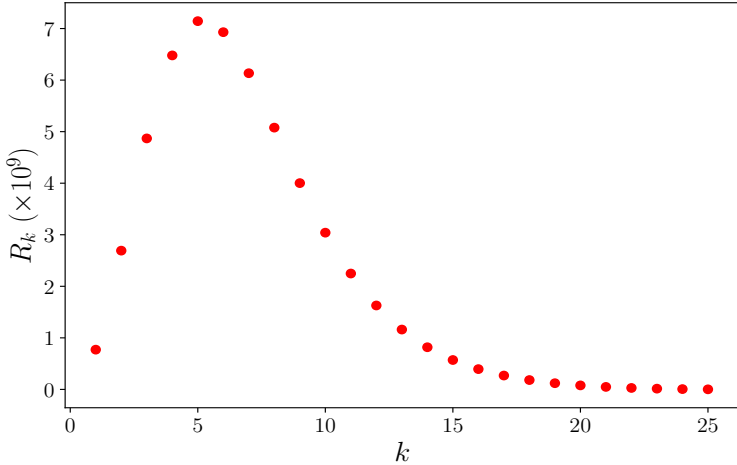


Figure 4: Plot of R_k for the individual Z'_k modes, where R_k denotes the dilepton production rate mediated by each Z'_k relative to the Z boson.

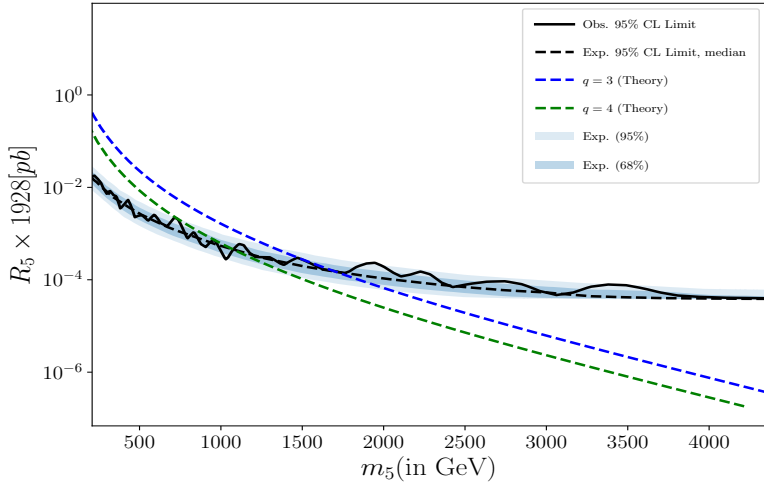


Figure 5: Comparison of R_5 (scaled by 1928 pb), as defined in Eq. (3.26), for two benchmark values $q = 3$ (blue dashed curve) and $q = 4$ (green dashed curve) for $N = 25$, with the 95% CL observed and expected limits from CMS dilepton searches at $\sqrt{s} = 13$ TeV and $L = 137 \text{ fb}^{-1}$. The blue bands denote the uncertainty, with the darker (lighter) shaded region corresponding to the 68% (95%) confidence level.

for the case of $N = 25$, it can be argued that these will be effectively valid for any N as the mode (k) yielding the largest signal strength will also accordingly vary.

At this stage, we turn to the dominant decay mode, namely $Z'_k \rightarrow \chi\bar{\chi}$. Since the χ is invisible, one must, instead, turn to a visible particle in the final state so as to trigger the detector. The lowest order processes leading to such a signal are $q + g \rightarrow \chi + \bar{\chi} + q$ or

$q + \bar{q} \rightarrow \chi + \bar{\chi} + g/\gamma$. The corresponding final state comprises a monojet (or monophoton) accompanied by missing transverse momentum, and is well-studied in the context of the LHC. Once again, the expected cross-sections are below the current sensitivities.

4 Dark matter phenomenology

Now that the model has been completely defined and its consistency with the standard EW physics established in terms of relevant constraints on its parameters, we have the requisite foundation to describe, in detail, the phenomenology of the DM candidate χ . It is clear from Eqs. (2.10) and (2.11) that the interactions of χ with the SM fermions are mediated by the photon, the Z boson, and the tower of heavy Z' s. As we have argued in Sec. (3), weak-scale CHAMPs must have only very feeble couplings with the photon and Z so as to be consistent with limits from the direct detection experiments, and this is naturally achieved via the clockwork mechanism. The primary mediators, then, are the Z' s that have unsuppressed (periodic) gauge couplings with χ as well as the SM fermions. As a result, the DM relic abundance in our setup is determined predominantly through the freeze-out mechanism. This entails the CHAMP decoupling from the SM bath once the temperature falls well below $T \sim m_\chi$ and eventually freezing-out as its rate of annihilation into the visible sector becomes comparable with that of the Hubble expansion¹¹.

Certain interesting phenomenological features characteristic to the clockwork portal emerge upon a careful investigation of the annihilation dynamics of the DM. This is best illustrated by assuming two distinct scenarios pertaining to the primary annihilation channels $\chi\bar{\chi} \rightarrow \psi\bar{\psi}$, $\chi\bar{\chi} \rightarrow Z'_k Z'_k$, and $\chi\bar{\chi} \rightarrow Z'_k \phi_n$, where ψ denotes the SM fermions. In the following, we first discuss in detail the case wherein only the SM channels are kinematically accessible and, thereafter, describe the more general case, including all possible channels.

4.1 The simplest scenario: $\chi\bar{\chi} \rightarrow \psi\bar{\psi}$

Annihilations to the SM particles dominate when $m_k, m_\phi \gtrsim 2m_\chi$ and the $H - \Phi_n$ mixings are small. Even within the SM channels, the fermionic final states dominate over the rest, namely the W^+W^- , ZZ and Zh channels. This can be simply understood from the fact that the $Z'WW$ couplings are induced through the $B^k - W^3$ mixings (post CWSB) and hence carry a v^2/f^2 suppression. Similarly, the subdominant nature of the Zh channel can be attributed to the $Z'Zh$ couplings that are suppressed by both a v^2/f^2 factor and the scalar mixing angle $\sin\zeta$. On the other hand, the t -channel annihilation to ZZ is trivially suppressed by the q^{-N} factor in the $Z\bar{\chi}\chi$ coupling.

The key difference between a generic Z' portal and the present case is manifested in the range of allowed DM masses consistent with the observed relic abundance. For a typical case of a Z' -portal, two qualitatively different situations prevail. Given that the DM is a cold gas, if $m_{Z'} \gtrsim 2m_\chi$, a resonance enhancement of the cross section (scaling as $g_{Z'}^2/m_{Z'}^2$) obtains and DM annihilation is rendered very efficient (occasionally, overly so). On the other hand, for a Z' far heavier (often the case in various scenarios), the cross section, away

¹¹If the cross sections are comparable to weak interaction ones, the freeze-out is expected to occur at a temperature $T_{fo} \sim m_\chi/20$.

from the resonance, would scale as $g_{Z'}^4 m_\chi^2 / m_{Z'}^4$. Reproducing the observed relic abundance, then, results, in either case, in a straightforward constraint in the parameter space. The said constraint, though, has to be examined against the bounds from direct (as well as indirect) searches.

The present case is more complicated. For one, unlike in canonical Z' models, the direct detection amplitudes here receives potentially significant contributions from photon exchanges, thereby affecting the said constraints. More importantly, we now have multiple Z' 's, all relatively closely spaced, with all the couplings determined by a single gauge coupling g_x . With g_x , in turn, being close to the SM hypercharge coupling—see Eq. (3.10)—the relic abundance is primarily determined by three parameters, *viz.* the DM mass, its charge Y_χ under $U(1)_N$ and the scale f (for it determines the Z' mass scale). There is also a residual dependence (q, N) through their influence on the masses of the Z' 's as well as their individual couplings to the fermions.

Close to the individual peaks ($m_\chi \sim m_k/2$), the corresponding amplitude suffers a large resonance enhancement, rendering the other contributions largely irrelevant. As with the single- Z' models, very close to resonance, the enhancement could be too strong thereby suppressing the relic abundance. Naturally, for two values of m_χ around $m_k/2$ the abundance would be just right. The exact distances from the central value would depend on the effective individual couplings of the Z' under question and, hence, its width. Away from the resonances, the situation is more complicated as the interference between the individual contributions become increasingly important. Two effects are in play here. As discussed in the preceding section, the couplings of the Z'_k oscillate with k , leading to potentially large cancellations between the amplitudes mediated by them. A further complication is that, unlike in the case of direct detection as discussed earlier, DM annihilation proceeds through s -channel diagrams and for $m_k^2 < s < m_{k+1}^2$ the two propagators have opposite signs. In other words, there is partial cancellation between diagrams with $m_k^2 < s$ owing to the oscillating nature of the couplings¹² And similar is the case for diagrams with $m_k^2 > s$. Finally, there is a further cancellation between the two subsets on account of the relative signs of the two sets of propagators.

Thus, effectively, the only contribution that matters in this case is the resonant annihilation of χ near any one of the Z' thresholds. The process has a dominant s -wave component and, hence, the corresponding thermally-averaged cross-section is, to the leading order, independent of $x^{-1} \equiv T/m_\chi$. Taking any one of the Z'_k as the mediator, and working in the limit where the light SM fermions are effectively massless (an excellent approximation), this is given by

$$\langle \sigma v \rangle_{CM} \approx \frac{(g^{\chi, k+1})^2 m_\chi^2 \left((g_V^{f, k+1})^2 + (g_A^{f, k+1})^2 \right)}{\pi (16m_\chi^4 - 8m_\chi^2 m_k^2 + m_k^4 + m_k^2 \Gamma_k^2)}, \quad (4.1)$$

where the various couplings are defined in Sec. (2) and Γ_k is the decay width of the Z'_k . Note that since the Z' 's and, hence, the heavy scalars ϕ 's, are phenomenologically required to have masses $\gtrsim 1$ TeV, they will generally decouple from the thermal bath pretty early and then promptly decay into the SM fermions.

¹²These are qualitatively similar to the t -channel cancellations shown in Sec. (3.2.2).

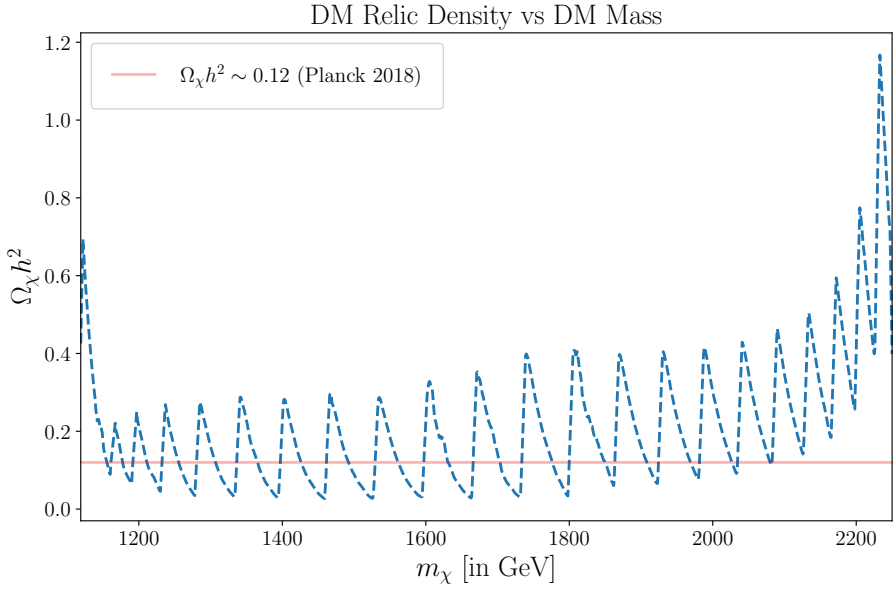


Figure 6: DM relic density (shown in dashed blue) for different values of its mass (as calculated with `MadDMv.3.2` [49, 50]) for the benchmark $N = 25$, $q = 3.0$, $f = 3$ TeV and $Y_\chi = 0.2$. The red line indicates the reference value of the observed relic abundance, $\Omega_\chi h^2 = 0.120 \pm 0.001$ [16]. Here, we focus on the most relevant region and show the variation only over a finite range of the DM mass where resonant annihilations through the Z' s dictate the DM yield, *i.e.* $m_\chi \in (m_1/2, m_N/2)$.

To illustrate the aforementioned dynamics with an example, we choose a configuration such that the CHAMP is potentially sensitive to the forthcoming DM direct detection experiments. This simply requires that the DM-nucleon cross-section be close to the current experimental limits for a given DM mass. Since collider constraints already imply $m_{Z'} \gtrsim 1$ TeV, we accordingly assume, for resonant annihilation, DM masses around similar scales. In compliance with the direct detection bounds we choose the parameter configuration $N = 25$, $q = 3.0$, and $f = 3$ TeV, for $Y_\chi = 0.2$, in which case the Z' spectrum appears with masses ranging from $2.2 - 4.6$ TeV. The correct relic abundance for χ can be achieved in this setup in the vicinity of the resonance regions, as shown in Fig. (6). Away from the resonances, the annihilation cross section is strongly suppressed due to the destructive interference in the total amplitude characteristic of the clockwork configuration, as discussed earlier, which leads to an overabundance of χ . However, resonance enhancement kicks in as the dark matter mass, m_χ , approaches the band of the CW Z' s, which results in a significant increase in the annihilation cross section. This, in turn, results in a sizable decline in the relic density. Consequently, the relic density curve exhibits a characteristic wavy pattern along the m_χ axis, which periodically coincides with the line corresponding to the correct relic abundance (shown in green), as seen in Fig. (6).

Looking more closely, the asymmetric shape of the relic density profile across the individual resonances, as seen in Fig. (6), can be well understood within the narrow width

approximation (NWA). In the NWA the thermally averaged annihilation cross section, in the limit that the SM fermion masses are negligible, can be approximated as [51]

$$\begin{aligned} \langle\sigma v\rangle &= \frac{1}{96 m_\chi^4 T K_2^2(m_\chi/T)} \sum_{k=1}^N (g^{\chi,k+1})^2 \left((g_V^{f,k+1})^2 + (g_A^{f,k+1})^2 \right) \\ &\times \frac{m_k (m_k^2 + 2m_\chi^2)}{\Gamma_k} \sqrt{(m_k^2 - 4m_\chi^2)} K_1\left(\frac{m_k}{T}\right) \theta(m_k - 2m_\chi), \end{aligned} \quad (4.2)$$

where $K_{1,2}$ are the modified Bessel functions of the first and the second kind, respectively. The Heaviside function rejects the contribution to $\langle\sigma v\rangle$ mediated by a particular Z'_k if the DM mass exceeds $m_k/2$. This, of course, is only an approximation as an off-shell Z'_k would contribute too. However, given the discussion above, it is easy to see that the cross section falls very fast away from the resonance. Consequently, for $m_\chi > m_k/2$, the contribution from that particular resonance may be well approximated to be vanishingly small since the minimum center-of-mass energy $\sqrt{s} = 2m_\chi$ exceeds m_k , making it impossible to hit the resonance. This inevitably results in a sharp rise of the relic density profile on one side of the resonance.

In contrast, for $m_\chi < m_k/2$, annihilation through the resonance still remains viable. In this case, the thermal motion of DM particles allows them to collide with sufficient energy to access the resonance region. This effect is captured by the thermal averaging procedure, where the momentum distribution of DM particles, encoded in the Bessel functions appearing in Eq. (4.2), ensures that a fraction of collisions occur at or near the resonance, thereby enhancing the annihilation cross section. This particular effect corresponds to the regions in the profile with a smooth variation near the individual resonances, as shown in Fig. (6).

4.2 Including all annihilation channels

In our discussions thus far, we have limited ourselves to DM annihilations into SM particles alone. This, of course, leads to an exact result as long as annihilations into the new particles are kinematically forbidden¹³. We now examine the consequences when this assumption no longer holds and other channels might be important too. This assumes importance as, for sufficiently large m_χ , the annihilation into the SM particles is no longer efficient enough to suppress the relic abundance down to the required level.

With the γ and Z couplings of the DM being very small, processes such as $\bar{\chi} + \chi \rightarrow Z'_k + Z/\gamma$ are of little interest, and the only relevant additional channels are those to $Z'_k + Z'_l$ and $Z'_k + \varphi_n$ respectively. We examine these in turn, and we only discuss the salient features here.

4.2.1 $\chi\bar{\chi} \rightarrow Z'_k Z'_l$

Kinematically accessible only when $2m_\chi > m_{Z'_k} + m_{Z'_l}$, these proceed through t -channel exchanges of χ itself. With a plethora of final states being available (at least for a sufficiently heavy χ), it might seem that the total annihilation cross section can be substantial. And with the Z' 's decaying promptly, this would be expected to suppress the relic abundance to

¹³Note that with the χ having only gauge couplings, co-annihilation processes are not possible.

a significant degree. However, it should be realised that couplings of the χ to the Z' 's all descend from a single one, *viz.* the $\bar{\chi}\chi X_N$ term and, in the unbroken phase, there would exist only the single process $\bar{\chi}\chi \rightarrow X_N + X_N$. Thus, in the limit of equal Z' masses,

$$\sum_{ij} \sigma(\chi\bar{\chi} \rightarrow Z'_k Z'_l) \simeq \sigma(\chi\bar{\chi} \rightarrow X_N X_N) ,$$

with the right hand side being evaluated in the absence of gauge boson mixing. In the above, the equality would be exact if the sum were to include the photon and the Z and, thus, the discrepancy is tiny indeed. The limit of equal Z' -masses, of course, does not hold. However, with the relative splittings being small, the above still continues to be a good approximation.

For the parameters chosen above, this extra contribution to DM annihilation is not sufficient. Indeed, with g_x being constrained to be very close to the hypercharge coupling within the SM, the $\bar{\chi}\chi \rightarrow X_N + X_N$ process can be enhanced only by either enhancing the $U(1)_N$ charge Y_χ or by reducing the Z' masses. The former alternative has an obvious limit from the requirement of perturbativity. More crucially, though, enhancing Y_χ indiscriminately would also increase the DM coupling with the photon, thereby coming into conflict with direct detection experiments. This, in turn, could be compensated for by increasing either q or N , with these being subject to various theoretical and experimental bounds as mentioned in Sec. (3). The second option, *viz.* making the Z' 's lighter, could, in principle, be achieved by lowering the clockwork scale f . However, $f \lesssim 1$ TeV is disfavoured from negative results for the dilepton searches.

It must be noted, though, that while the $Z'Z'$ channel, by itself, is largely insufficient in yielding the correct DM abundance for a large portion of the parameter space, it is quite possible that other channels compensate for the required cross-section. The contributions of the remaining channels to this effect are examined in the following.

4.2.2 $\chi\bar{\chi} \rightarrow Z'_k \varphi_n, Z'_k \Phi$

With all the putative pseudoscalars being absorbed by the gauge bosons, the only remaining possibilities are the Bjorken-process analogues (*viz.*, $\chi\bar{\chi} \rightarrow Z'_k \varphi_n, Z'_k \Phi$) that open up for $2m_\chi \gtrsim m_k + m_\varphi$ and $2m_\chi \gtrsim m_k + m_\Phi$ respectively. The scalar masses—see Eq. (3.5)—are governed by the two essentially free parameters ξ and η in the potential—see Eq. (3.1)—with the only constraint being observability at the LHC (as highlighted in Sec. (3)).

Once again, the plethora of possible final states is misleading as, above the clockwork scale, the only relevant annihilation amplitude is $\chi\bar{\chi} \rightarrow X_N \phi_{N-1}$ and all the amplitudes discussed above descend from this single one. In terms of the mass eigenstates (φ_n, Φ) , nondiagonal vertices $Z'_k Z'_l \varphi_n$ etc. exist and the individual annihilation processes are, in principle, mediated by all the Z' 's. Consequently, an analogue of the destructive inference operative for the fermionic channel also holds here, albeit with the cancellations becoming less significant as $k \rightarrow N$.

Nevertheless, the $Z'\varphi$ annihilation channels, combined with the $Z'Z'$ ones, can indeed yield the typical WIMP DM cross-section $\langle\sigma v\rangle_{\text{ann}} \sim 10^{-26} \text{ cm}^3/\text{s}$, provided $m_{Z'}, m_\varphi \lesssim 1$ TeV. Since the latter requirement invariably translates to $f \lesssim 1$ TeV, only a small region

of the parameter space remains viable for a DM candidate, consistent with the other constraints. For instance, one such allowed configuration goes as — $m_\chi \sim 1.5$ TeV, $Y_\chi \sim \mathcal{O}(1)$, $f \sim 1$ TeV ($m_k^{\max} \sim 2$ TeV), $m_\varphi \sim 1$ TeV, $q = 4$ and $N \sim 20$.

In conclusion, it is perhaps worth drawing a qualitative comparison of the nonresonant annihilation to Z'/φ with the resonant annihilation to the SM fermions. Since the success of the combination of the $Z'_k Z'_l$ and $Z'_k \varphi_n$ channels in setting the correct DM abundance is contingent on the Z' and φ masses being close to the current experimental bounds, and having $U(1)$ charges near perturbative thresholds, the scenario is imminently and independently falsifiable from future electroweak precision measurements as well as dedicated Z' and heavy Higgs searches. In contrast, the $f\bar{f}$ channel becomes relevant only at the Z'_k resonances and, hence, is very characteristic of the clockwork portal. Thus, even if the next generation of direct-detection experiments place stricter limits on the DM-nucleon cross-section, or future Z' searches push the lower limit on their masses beyond the multi-TeV range, the resonance portal would still allow for a natural realization of a CHAMP DM as it only requires a modification in q and N , alongwith with the assumption little hierarchy between v and f .

5 Summary and Discussion

We revisit the possibility of an electrically charged dark matter candidate for the highly constrained, and hitherto less-explored, case of a near weak-scale charged massive particle (CHAMP). To realize a scenario with no unnaturally small parameters, we invoke a gauged *clockwork* portal mediating the dark and the visible sectors, which not only helps generate the required suppression in the electric charge of the DM but also serves to determine the correct DM relic abundance through a freeze-out mechanism. The clockwork sector comprises $(N+1)$ copies of an Abelian gauge field, with N complex scalars suitably charged so as to act as *links* between adjacent gauge fields, exhibiting a lattice structure with only nearest-neighbour interactions. Resorting to the most minimal picture, we invoke this sector as an extension of the SM hypercharge ($U(1)_Y \rightarrow U(1)^{N+1}$) such that the zero mode of the spectrum, post the spontaneous breaking of the clockwork sector symmetry, emulates the SM boson B_μ . In the physical basis, then, this results in the photon being intertwined with the CW sector—rather than a purely SM entity—with an exponentially falling distribution over the CW lattice. With the SM particles charged under $U(1)_0$ and the CHAMP charged under $U(1)_N$, this leads to the photon having the usual $\mathcal{O}(1)$ couplings with the SM particles and a q^{-N} -suppressed interaction with the DM. Thus, for $q > 1$, the DM can be made to effectively carry a very tiny electric charge, even if we assign an $\mathcal{O}(1)$ charge to it under $U(1)_N$.

For simplicity, and to avoid complications related to anomalies, we assume the DM field (χ) to be a single vector-like Dirac fermion, which trivially renders it stable. It interacts with the visible sector dominantly through the N heavy Z 's present in the CW spectrum (with the couplings being mandated by the gauge boson mixings engendered by the CW mechanism), whose masses are determined by the SSB scale $f(\gg v)$. The DM abundance is then set by a conventional freeze-out mechanism, dictated by DM annihilation to the

SM particles. To this effect, the most accessible channel in terms of the available parameter space turns out to be the Z' mediated annihilation to the SM fermions. The correct relic density is reached only when $m_\chi \sim m_{Z'}/2$, for any Z' , since away from the poles the individual Z' -mediated contributions destructively interfere and undergo severe cancellations. This sets a characteristic scale for the DM mass in the model, inevitably tied to the symmetry breaking scale f .

Although, naively, a setup as such might seem *ad hoc* and overtly complicated in nature, it is important to note that it can possibly be viewed as a deconstruction of a five-dimensional braneworld scenario wherein the hypercharge gauge boson is placed in the bulk. In that case, the rest of the SM fields and the DM should be localized on the IR and the UV branes, respectively. The relevant geometry, as suggested in ref.[28], can be generated by a linear dilaton augmentation of 5D gravity [52, 53].

The most important theoretical constraint on the setup is due to the scalar potential stability and reads $N\eta < \lambda\xi$. However, phenomenologically, the most relevant bounds on the model arise from experimental observations. For instance, the current upper limit on the DM-nucleon scattering cross-section, from LUX-ZEPLIN places the most stringent upper bound on the electric charge of the DM ($\sim 10^{-12}$). Since even for the t -channel processes the individual Z' contributions effectively cancel out due to the periodic nature of the couplings, the DM-nucleon scattering in the model proceeds primarily through a photon exchange and, therefore, the aforementioned bound directly limits the combination q^{-N} . On the other hand, negative results for dilepton searches translate to a lower bound on the Z' mass scale, namely $m'_{Z'} \gtrsim \mathcal{O}(1)$ TeV, which happens to be stronger than the bounds derived from direct searches at the LHC (for effective couplings as applicable to this model).

The clockwork portal scenario for a CHAMP stands out in two major aspects. Firstly, unlike in typical WIMP models, demanding consistency with persistent null results at the direct detection experiments in the future will not necessarily render the model unnatural. This is simply because the required suppression in the rates can always be accommodated by adjusting the number of portal fields N accordingly (and perhaps also marginally increasing the hopping charge q within the perturbativity limits). While this might seem uninteresting in terms of the testability of the model, it nevertheless exhibits robustness against the potentially tightening constraints from the next generation of direct search experiments. Secondly, since the most relevant case of a viable DM involves resonant annihilations to SM fermions, the masses of the heavy mediators (*i.e.* the Z' 's) are neither constrained from the required DM yield, nor from the stringent direct detection limits as the DM-nucleon scatterings are dominated by photon exchanges alone. Therefore, a plausible CHAMP scenario, with TeV scale masses for both the DM and the heavy mediators, seems quite straightforwardly achievable in this setup. There is a caveat, though, to both the arguments above. While increasing q^N does suppress the photon exchange contribution to the direct detection cross sections, the heavy gauge mediated contributions remain largely unaffected and, thus, future experiments would still be able to probe the model, albeit in a more traditional mode. Moreover, the increased q^N suppression has little effect on the electroweak precision observables. Consequently, the model would remain eminently testable at a FCC-

ee machine, with a projected goal of producing $\gtrsim 10^{12}$ Z -bosons.

Since the DM in the setup favours annihilations into a pair of charged fermions through a Z' , it is potentially sensitive to an array of forthcoming (or planned) MeV scale γ -ray telescopes such as AMEGO [54–56], E-ASTROGAM [57, 58] and MAST [59], which are expected to target weak-scale DM candidates as well. Even without a dedicated study of the γ -ray fluxes within the model, a qualitative inference can be sought from the model-independent analysis in ref.[30] of the sensitivity projections of the aforementioned experiments for a weak-scale DM. Of course, a direct or indirect signal of a weak-scale DM would not necessarily reveal the nature of the portal as well. Conservatively, then, only a direct search for the multi- Z' (and the accompanying multi-scalar) spectrum can qualify as a probe of the clockwork portal. Given the allowed mass scale of the Z 's in the TeV range or beyond, some of the proposed or planned collider experiments in the high-luminosity (*e.g.* HL-LHC) or the high-energy frontiers (*e.g.* FCC-hh, multi-TeV muon collider, etc.) would serve as ideal discovery grounds for such a scenario.

Acknowledgement

DC acknowledges the ANRF, Government of India, for support through the project CRG/2023/008234 and the IoE, University of Delhi grant IoE/2025-26/12/FRP. V.K.J. acknowledges financial support provided by the UGC, Government of India. S.M. would like to thank Prolay K. Chanda for helpful discussions. S.M. also acknowledges support from the Department of Atomic Energy (Government of India).

References

- [1] A. De Simone, G.F. Giudice and A. Strumia, *Benchmarks for Dark Matter Searches at the LHC*, *JHEP* **06** (2014) 081 [[1402.6287](#)].
- [2] G. Arcadi, Y. Mambrini and F. Richard, *Z-portal dark matter*, *JCAP* **03** (2015) 018 [[1411.2985](#)].
- [3] P. Chanda, S. Hamdan and J. Unwin, *Reviving Z and Higgs Mediated Dark Matter Models in Matter Dominated Freeze-out*, *JCAP* **01** (2020) 034 [[1911.02616](#)].
- [4] M. Escudero, A. Berlin, D. Hooper and M.-X. Lin, *Toward (Finally!) Ruling Out Z and Higgs Mediated Dark Matter Models*, *JCAP* **12** (2016) 029 [[1609.09079](#)].
- [5] A. De Rujula, S.L. Glashow and U. Sarid, *CHARGED DARK MATTER*, *Nucl. Phys. B* **333** (1990) 173.
- [6] M.I. Dobroliubov and A.Y. Ignatiev, *MILLICHARGED PARTICLES*, *Phys. Rev. Lett.* **65** (1990) 679.
- [7] S. Dimopoulos, D. Eichler, R. Esmailzadeh and G.D. Starkman, *Getting a Charge Out of Dark Matter*, *Phys. Rev. D* **41** (1990) 2388.
- [8] G. Magill, R. Plestid, M. Pospelov and Y.-D. Tsai, *Millicharged particles in neutrino experiments*, *Phys. Rev. Lett.* **122** (2019) 071801.
- [9] A. Haas, C.S. Hill, E. Izaguirre and I. Yavin, *Looking for milli-charged particles with a new experiment at the LHC*, *Phys. Lett. B* **746** (2015) 117 [[1410.6816](#)].
- [10] MINIBooNE collaboration, *Significant Excess of ElectronLike Events in the MiniBooNE Short-Baseline Neutrino Experiment*, *Phys. Rev. Lett.* **121** (2018) 221801 [[1805.12028](#)].
- [11] K.J. Kelly and Y.-D. Tsai, *Proton fixed-target scintillation experiment to search for millicharged dark matter*, *Phys. Rev. D* **100** (2019) 015043 [[1812.03998](#)].
- [12] S. Davidson, S. Hannestad and G. Raffelt, *Updated bounds on millicharged particles*, *JHEP* **05** (2000) 003 [[hep-ph/0001179](#)].
- [13] A. Badertscher, P. Crivelli, W. Fettscher, U. Gendotti, S.N. Gninenko, V. Postoev et al., *Improved limit on invisible decays of positronium*, *Phys. Rev. D* **75** (2007) 032004.
- [14] A.A. Prinz, R. Baggs, J. Ballam, S. Ecklund, C. Fertig, J.A. Jaros et al., *Search for millicharged particles at slac*, *Phys. Rev. Lett.* **81** (1998) 1175.
- [15] G.G. Raffelt, *Stars as laboratories for fundamental physics: The astrophysics of neutrinos, axions, and other weakly interacting particles* (5, 1996).
- [16] PLANCK collaboration, *Planck 2018 results. VI. Cosmological parameters*, *Astron. Astrophys.* **641** (2020) A6 [[1807.06209](#)].
- [17] L. Chuzhoy and E.W. Kolb, *Reopening the window on charged dark matter*, *JCAP* **07** (2009) 014 [[0809.0436](#)].
- [18] D. Dunsky, L.J. Hall and K. Harigaya, *CHAMP Cosmic Rays*, *JCAP* **07** (2019) 015 [[1812.11116](#)].
- [19] PARTICLE DATA GROUP collaboration, *Review of particle physics*, *Phys. Rev. D* **110** (2024) 030001.
- [20] S.D. McDermott, H.-B. Yu and K.M. Zurek, *Turning off the Lights: How Dark is Dark Matter?*, *Phys. Rev. D* **83** (2011) 063509 [[1011.2907](#)].

[21] T. Gherghetta, J. Kersten, K. Olive and M. Pospelov, *Evaluating the price of tiny kinetic mixing*, *Phys. Rev. D* **100** (2019) 095001 [[1909.00696](#)].

[22] S.A. Abel and B.W. Schofield, *Brane anti-brane kinetic mixing, millicharged particles and SUSY breaking*, *Nucl. Phys. B* **685** (2004) 150 [[hep-th/0311051](#)].

[23] S.A. Abel, M.D. Goodsell, J. Jaeckel, V.V. Khoze and A. Ringwald, *Kinetic Mixing of the Photon with Hidden $U(1)$ s in String Phenomenology*, *JHEP* **07** (2008) 124 [[0803.1449](#)].

[24] M. Goodsell, J. Jaeckel, J. Redondo and A. Ringwald, *Naturally Light Hidden Photons in LARGE Volume String Compactifications*, *JHEP* **11** (2009) 027 [[0909.0515](#)].

[25] K. Choi, H. Kim and S. Yun, *Natural inflation with multiple sub-Planckian axions*, *Phys. Rev. D* **90** (2014) 023545 [[1404.6209](#)].

[26] D.E. Kaplan and R. Rattazzi, *Large field excursions and approximate discrete symmetries from a clockwork axion*, *Phys. Rev. D* **93** (2016) 085007 [[1511.01827](#)].

[27] K. Choi and S.H. Im, *Realizing the relaxion from multiple axions and its UV completion with high scale supersymmetry*, *JHEP* **01** (2016) 149 [[1511.00132](#)].

[28] G.F. Giudice and M. McCullough, *A Clockwork Theory*, *JHEP* **02** (2017) 036 [[1610.07962](#)].

[29] H.M. Lee, *Gauged $U(1)$ clockwork theory*, *Phys. Lett. B* **778** (2018) 79 [[1708.03564](#)].

[30] M. Cirelli and A. Kar, *Prospects of future MeV telescopes in probing weak-scale dark matter*, *SciPost Phys.* **19** (2025) 080 [[2503.04907](#)].

[31] H. Georgi, *A Tool Kit for Builders of Composite Models*, *Nucl. Phys. B* **266** (1986) 274.

[32] A.E. Nelson, *CONSTRAINTS ON MOOSE MODEL BUILDING*, *Phys. Lett. B* **167** (1986) 200.

[33] I. Rothstein and W. Skiba, *Mother Moose: generating extra dimensions from simple groups at large N* , *Phys. Rev. D* **65** (2002) 065002 [[hep-th/0109175](#)].

[34] N. Arkani-Hamed, A.G. Cohen, E. Katz, A.E. Nelson, T. Gregoire and J.G. Wacker, *The Minimal moose for a little Higgs*, *JHEP* **08** (2002) 021 [[hep-ph/0206020](#)].

[35] T. Gregoire and J.G. Wacker, *Moosees, topology and Higgs*, *JHEP* **08** (2002) 019 [[hep-ph/0206023](#)].

[36] T. Robens and T. Stefaniak, *LHC Benchmark Scenarios for the Real Higgs Singlet Extension of the Standard Model*, *Eur. Phys. J. C* **76** (2016) 268 [[1601.07880](#)].

[37] T. Appelquist, B.A. Dobrescu and A.R. Hopper, *Nonexotic Neutral Gauge Bosons*, *Phys. Rev. D* **68** (2003) 035012 [[hep-ph/0212073](#)].

[38] G.M. Pruna and T. Robens, *Higgs singlet extension parameter space in the light of the LHC discovery*, *Phys. Rev. D* **88** (2013) 115012 [[1303.1150](#)].

[39] T. Robens and T. Stefaniak, *Status of the Higgs Singlet Extension of the Standard Model after LHC Run 1*, *Eur. Phys. J. C* **75** (2015) 104 [[1501.02234](#)].

[40] F. Bojarski, G. Chalons, D. Lopez-Val and T. Robens, *Heavy to light Higgs boson decays at NLO in the Singlet Extension of the Standard Model*, *JHEP* **02** (2016) 147 [[1511.08120](#)].

[41] T. Robens and R. Santos, *BSM: Extended Scalar Sectors*, 7, 2025 [[2507.21910](#)].

[42] F. Feuerstake, E. Fuchs, T. Robens and D. Winterbottom, *Interference effects in resonant*

*di-Higgs production at the LHC in the Higgs singlet extension, *JHEP* **04** (2025) 094* [[2409.06651](#)].

[43] ALEPH, DELPHI, L3, OPAL, LEP ELECTROWEAK WORKING GROUP collaboration, *A Combination of preliminary electroweak measurements and constraints on the standard model*, [hep-ex/0612034](#).

[44] E. Iles, S. Heeba and K. Schutz, *Dark Matter Direct Detection Experiments Are Sensitive to the Millicharged Background*, *Phys. Rev. Lett.* **134** (2025) 121002 [[2407.21096](#)].

[45] LZ collaboration, *Dark Matter Search Results from 4.2 Tonne-Years of Exposure of the LUX-ZEPLIN (LZ) Experiment*, *Phys. Rev. Lett.* **135** (2025) 011802 [[2410.17036](#)].

[46] CMS collaboration, *Search for resonant and nonresonant new phenomena in high-mass dilepton final states at $\sqrt{s} = 13$ TeV*, *JHEP* **07** (2021) 208 [[2103.02708](#)].

[47] R. Hamberg, W.L. van Neerven and T. Matsuura, *A complete calculation of the order α_s^2 correction to the Drell-Yan K factor*, *Nucl. Phys. B* **359** (1991) 343.

[48] ATLAS collaboration, *Search for new high-mass phenomena in the dilepton final state using 36 fb^{-1} of proton-proton collision data at $\sqrt{s} = 13$ TeV with the ATLAS detector*, *JHEP* **10** (2017) 182 [[1707.02424](#)].

[49] M. Backovic, K. Kong and M. McCaskey, *MadDM v.1.0: Computation of Dark Matter Relic Abundance Using MadGraph5*, *Physics of the Dark Universe* **5-6** (2014) 18 [[1308.4955](#)].

[50] M. Backović, A. Martini, O. Mattelaer, K. Kong and G. Mohlabeng, *Direct Detection of Dark Matter with MadDM v.2.0*, *Phys. Dark Univ.* **9-10** (2015) 37 [[1505.04190](#)].

[51] P. Gondolo and G. Gelmini, *Cosmic abundances of stable particles: Improved analysis*, *Nuclear Physics B* **360** (1991) 145.

[52] I. Antoniadis, A. Arvanitaki, S. Dimopoulos and A. Giveon, *Phenomenology of TeV Little String Theory from Holography*, *Phys. Rev. Lett.* **108** (2012) 081602 [[1102.4043](#)].

[53] P. Cox and T. Gherghetta, *Radion Dynamics and Phenomenology in the Linear Dilaton Model*, *JHEP* **05** (2012) 149 [[1203.5870](#)].

[54] AMEGO collaboration, *All-sky Medium Energy Gamma-ray Observatory: Exploring the Extreme Multimessenger Universe*, [1907.07558](#).

[55] C.A. Kierans, *AMEGO: exploring the extreme multimessenger universe*, in *Society of Photo-Optical Instrumentation Engineers (SPIE) Conference Series*, J.-W.A. den Herder, S. Nikzad and K. Nakazawa, eds., vol. 11444 of *Society of Photo-Optical Instrumentation Engineers (SPIE) Conference Series*, p. 1144431, Jan., 2021, DOI [[2101.03105](#)].

[56] R. Caputo et al., *All-sky Medium Energy Gamma-ray Observatory eXplorer mission concept*, *J. Astron. Telesc. Instrum. Syst.* **8** (2022) 044003 [[2208.04990](#)].

[57] e-ASTROGAM collaboration, *The e-ASTROGAM mission*, *Exper. Astron.* **44** (2017) 25 [[1611.02232](#)].

[58] e-ASTROGAM collaboration, *Science with e-ASTROGAM: A space mission for MeV-GeV gamma-ray astrophysics*, *JHEAp* **19** (2018) 1 [[1711.01265](#)].

[59] T. Dzhatdoev and E. Podlesnyi, *Massive Argon Space Telescope (MAST): A concept of heavy time projection chamber for γ -ray astronomy in the 100 MeV-1 TeV energy range*, *Astropart. Phys.* **112** (2019) 1 [[1902.01491](#)].